Dalton Transactions

ROYAL SOCIETY OF CHEMISTRY

PAPER

View Article Online
View Journal | View Issue

Cite this: *Dalton Trans.*, 2025, **54**, 6495

Exploring a series of multifunctional Mn(I) tricarbonyls as prospective agents against trypanosomatid parasites: a comparative study with the Re(I) analogues†

Carolina Del Mármol, [a,b,c] Gonzalo Scalese, [a] Rodrigo Moreira, [a,b,c] Nicolás Veiga, [a] Ignacio Machado, [d] Ricardo Faccio, [e] Analía Lima, [f,g] Rosely A. Peralta, [h] Leticia Pérez-Díaz [i] and Dinorah Gambino *[a]

Diseases caused by trypanosomatid parasites are among the most pressing neglected illnesses. Chagas disease, caused by *Trypanosoma cruzi*, and visceral Leishmaniasis, caused by *Leishmania infantum*, have a severe health impact in developing countries. Searching for prospective metal-based drugs against these diseases, five multifunctional *fac*-[Mn(CO)$_3$(CTZ)(NN)](PF$_6$) compounds, including four new derivatives, were synthesized and thoroughly characterized, featuring NN polypyridyl derivatives and Clotrimazole (CTZ) as bioactive ligands. The biological behavior was compared with that previously reported for the Re analogues. Mn compounds showed EC$_{50}$ values in the low micromolar range against the infective trypomastigote form of *Trypanosoma cruzi* and the promastigote form of *Leishmania infantum* and moderate selectivity indexes. While their potency against *T. cruzi* was comparable to the Re analogues, their selectivity was lower. Key physicochemical properties relevant to drug development were assessed: Mn(I) compounds showed lower stability in relevant tested media compared with their Re(I) counterparts and higher lipophilicity than the free ligands and the Re analogues. To gain insight into the potential mechanisms of action, the interaction with DNA and the effects on ergosterol biosynthesis in *T. cruzi* and *L. infantum* were investigated. Minimal DNA association (<1%) and moderate interaction with this target discarded DNA binding as the primary mechanism of action. In contrast, inhibition of lanosterol 14-α-demethylase (CYP51), key enzyme involved in the parasites' ergosterol biosynthetic pathway, was experimentally confirmed. Metallomic study revealed an uptake by *T. cruzi* of the most promising compound, *fac*-[Mn(CO)$_3$(CTZ)(tmp)](PF$_6$), more than twice that of the Re(I) analogue and preferential association to soluble proteins. Proteomic analysis of *T. cruzi* epimastigotes treated with the Mn(I) and Re(I) analogues showed no change in CYP51 abundance, suggesting that reduced ergosterol levels may arise from post-translational modifications of the enzyme. Raman confocal microscopy allowed us to detect effects of the most promising Mn compound in treated *T. cruzi*. Furthermore, the photoinduced CO release properties of both Mn and Re analogues were examined, searching for an additional and yet non-studied potential mechanism of action of metal-tricarbonyls in these trypanosomatid parasites. Collectively, the results highlight the potential of Mn(I) tricarbonyls as promising candidates for further drug development.

Received 29th January 2025,
Accepted 9th March 2025

DOI: 10.1039/d5dt00241a

rsc.li/dalton

[a]*Área Química Inorgánica, DEC, Facultad de Química, Universidad de la República, Uruguay. E-mail: dgambino@fq.edu.uy; Fax: +5982-9241906; Tel: +5982-9249739*
[b]*Programa de Posgrado de Facultad de Química, Universidad de la República, Uruguay*
[c]*PEDECIBA – Programa de Desarrollo de las Ciencias Básicas, Uruguay*
[d]*Área Química Analítica, DEC, Facultad de Química, Universidad de la República, Uruguay*
[e]*Área Física, DETEMA, Facultad de Química, Universidad de la República, Uruguay*
[f]*Unidad de Bioquímica y Proteómica Analíticas, Institut Pasteur de Montevideo, Uruguay*
[g]*Instituto de Investigaciones Biológicas Clemente Estable, Uruguay*
[h]*Departamento de Química, Universidade Federal de Santa Catarina, Florianópolis, Brazil*
[i]*Sección Genómica Funcional, Facultad de Ciencias, Universidad de la República, Uruguay*

† Electronic supplementary information (ESI) available. See DOI: https://doi.org/10.1039/d5dt00241a

Introduction

Neglected tropical diseases (NTDs) comprise a diverse set of twenty medical conditions, identified by the World Health Organization (WHO) as such, caused by various pathogens, including viruses, bacteria, protozoa, and parasitic worms. These diseases primarily affect impoverished populations living in tropical regions, afflicting more than 1 billion people across 149 countries. Most drugs used to treat NTDs are outdated and often cause unwanted side effects. Unfortunately, pharmaceutical companies show limited interest in developing new treatments or vaccines for these diseases since the affected population mainly resides in low-income regions, which anticipates low financial returns. Consequently, much of the research on NTDs is driven by academic institutions, open-source initiatives, and nonprofit organizations.[1–6]

Diseases caused by trypanosomatid parasites—such as Human African Trypanosomiasis, Chagas disease, and Leishmaniasis—are among the most pressing neglected illnesses, creating a severe health crisis in developing countries. Chagas disease, also known as American Trypanosomiasis, is an ancient endemic illness in Latin America caused by the flagellated protozoa *Trypanosoma cruzi* (*T. cruzi*). Currently, around 6–7 million people are infected, with Chagas disease burden estimated to be five times that of malaria. In this region, the parasite typically spreads to mammals through the bite of infected, blood-feeding triatomine bugs. In recent decades, the migration flow to areas like North America, Australia, Europe, and Japan has led to increased cases in these non-endemic regions, with transmission occurring through routes such as blood transfusions, organ transplants, and mother-to-child transmission.[7] Leishmaniasis, in turn, is caused by over 20 species of *Leishmania*. These parasites are transmitted to mammalian hosts through bites of female phlebotomine sandflies. Present in 98 countries worldwide, leishmaniasis poses a risk to more than 1 billion people living in endemic areas pertaining to most continents, with the WHO reporting an estimate of more than 1 million new cases annually. Visceral leishmaniasis, produced by *L. infantum*, is the most severe form of the disease, leading to death if untreated.[7–13]

Despite notable differences between both trypanosomatid protozoan parasites—including their transmission by different insect vectors and the diverse clinical diseases they cause—research has revealed significant similarities in their biology, sharing closely related protein-encoding genes. This fact creates opportunities to develop broad-spectrum compounds, potentially affecting common targets in both parasites.[14–17]

In recent decades, research in inorganic medicinal chemistry has advanced in the development of potential new drugs against trypanosomatid parasites.[3,4,18–27] In this field, our group's current strategy focuses on the rational design of multifunctional classical metal compounds and organometallics, achieved by hybridizing various pharmacophoric entities. This approach involves integrating a bioactive or pharmacologically relevant metal center, bioactive organic ligands—compounds with demonstrated antitrypanosomatid activity—and, where necessary, suitable co-ligands into a single hybrid compound. This design strategy has frequently produced multifunctional compounds with multiple modes of action and good to high selectivity toward the parasites.[4,28–32]

In this framework, we recently reported promising results on the rational design of multifunctional Re(I) tricarbonyl compounds with two different bioactive ligands, *fac*-$[Re(CO)_3(CTZ)(NN)](PF_6)$, where CTZ is Clotrimazole and NN represents a series of polypyridyl derivatives of 1,10-phenanthroline or 2,2′-bipyridine, as prospective anti *T. cruzi* agents.[29,33] Re(I) tricarbonyl compounds offer notable advantages for applications in medicinal chemistry. The *fac*-$[Re^{I}(CO)_3]^{+}$ core is both chemically robust and readily accessible *via* straightforward synthetic routes.[34] This class of compounds has been extensively explored for their potential in cancer therapy, as agents in nuclear medicine and as bactericidals, while the research as antiparasitic compounds has been primarily limited to cyrhetrenyl derivatives, some complexes of bioactive semicarbazones and thiosemicarbazones reported by our group and a recent report on Re(I)–Tc(I) megazol derivatives.[34–45]

The chosen azole, CTZ, inhibits the activity of lanosterol 14-alpha-demethylase (CYP51), an enzyme responsible for converting lanosterol into zymosterol, a precursor of ergosterol. Ergosterol, the primary sterol in trypanosomatid parasites, plays a critical role in maintaining membrane structure and function, as well as supporting parasite replication.[46–48] The selected bidentate NN ligands have demonstrated activity against *T. cruzi*. Their intercalative properties may be transferred to their complexes, suggesting DNA as a potential molecular target.[49–51]

Manganese, the congener of rhenium, is an essential metal present in the active sites of various enzymes. Its biological relevance could suggest that replacing rhenium with manganese in coordination compounds could yield compounds with reduced toxicity. However, manganese compounds remain relatively underexplored in inorganic medicinal chemistry. A few reported Mn(II) compounds have shown potential applications as anticancer, antibacterial, and antifungal agents, as well as imaging contrast agents.[52,53] Compounds featuring the *fac*-$[Mn^{I}(CO)_3]$ core have been investigated as carbon monoxide-releasing molecules (CORMs) with antibacterial activity, leveraging the therapeutic potential of CO.[54–59]

However, research on the activity of Mn(I) tricarbonyl compounds against trypanosomatid parasites remains limited to few studies.[60,61]

In this study, five *fac*-$[Mn(CO)_3(CTZ)(NN)](PF_6)$ compounds, including four newly synthesized ones, featuring the NN ligands depicted in Fig. 1, were successfully synthesized and thoroughly characterized. Their biological activity was evaluated against *T. cruzi* epimastigotes and trypomastigotes, *L. infantum* promastigotes, and VERO cells as a mammalian cell model. Additionally, key physicochemical properties relevant to drug development, such as lipophilicity and solution stability in various media, were assessed. To gain insight into the potential mechanisms of action of the compounds, their

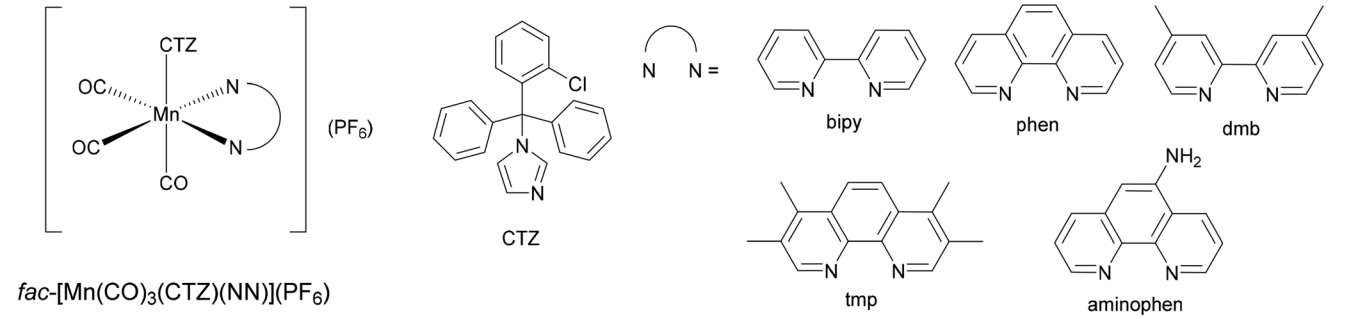

Fig. 1 Structures of the *fac*-$[Mn(CO)_3(CTZ)(NN)](PF_6)$, where CTZ is Clotrimazole and NN is a polypyridyl derivative of 1,10-phenanthroline or 2,2′-bipyridine. bipy: 2,2′-bipyridine; dmb: 4,4′-dimethyl-2,2′-bipyridine; phen: 1,10-phenanthroline; tmp: 3,4,7,8-tetramethyl-1,10-phenanthroline; aminophen: 5-amino-1,10-phenanthroline.

interactions with DNA and their effects on ergosterol biosynthesis in *T. cruzi* and *L. infantum* were experimentally investigated. Omics approaches were employed, including metallomic analyses to determine compound uptake and association with selected biomolecular fractions in *T. cruzi* epimastigotes, as well as proteomic studies. Raman confocal microscopy allowed us to detect effects of the most promising compound in treated *T. cruzi* parasites. The whole set of results was compared with those obtained for previously reported Re analogues.[29] Furthermore, the photoinduced CO release properties of both Mn and Re compounds were examined, searching for an additional and yet non-studied potential mechanism of action in trypanosomatid parasites.

Experimental section

General considerations

All chemical reagents were obtained from commercial sources and used without further purification. All reactions were performed under N_2 atmosphere, strictly protected from light and using degassed solvents. The analogous *fac*-$[Re(CO)_3(CTZ)(NN)](PF_6)$ compounds were synthesized and characterized as previously reported by us.[29,33]

Chemical and physical measurements

C, N and H analyses were performed with a Thermo Scientific Flash 2000 elemental analyzer. FTIR spectra were measured as KBr pellets with a Shimadzu IR Prestige-21 instrument, and as CH_2Cl_2 solution with a PerkinElmer Spectrum 100 FT-IR spectrophotometer with a CaF_2 cell. ^1H and ^{31}P-NMR spectra were recorded in DMSO-d_6 at 25 °C on a Bruker Avance NEO DPZ-400 instrument at 400 MHz and 162 MHz, respectively. Bi-dimensional COSY experiments were carried out with the same instrument. Residual peaks of DMSO were used as the internal standard and chemical shifts are reported in ppm and coupling constants in Hz. Electronic spectra were measured with a Varian Cary 50 BIO UV-Vis spectrometer, employing a quartz cuvette with a 1.0 cm path length and spectroscopy-grade solvents.

Synthesis of the *fac*-$[Mn(CO)_3(CTZ)(NN)](PF_6)$ compounds

The complexes were synthesized through a four-stepped procedure depicted in Fig. 2. Briefly, $[MnBr(CO)_5]$ and the stoichiometric amount of NN ligand were suspended in CH_2Cl_2, and stirred for 24 h. The solid *fac*-$[MnBr(CO)_3(NN)]$ compounds obtained were washed and dried. Equimolar amounts of silver triflate, AgOTf, and *fac*-$[MnBr(CO)_3(NN)]$ were suspended in acetone and stirred for 3 h. The suspension, containing solid AgBr, was centrifuged and the supernatant was separated, evaporated under reduced pressure and resuspended in MeOH. Subsequently, an equimolar amount of Clotrimazole (CTZ) was added to the suspension and stirred for 24 h. $NaPF_6$ was added in 100% excess and the mixture was stirred for 24 h. The final compound was isolated by centrifugation, washed and dried in a vacuum drying bell jar system.

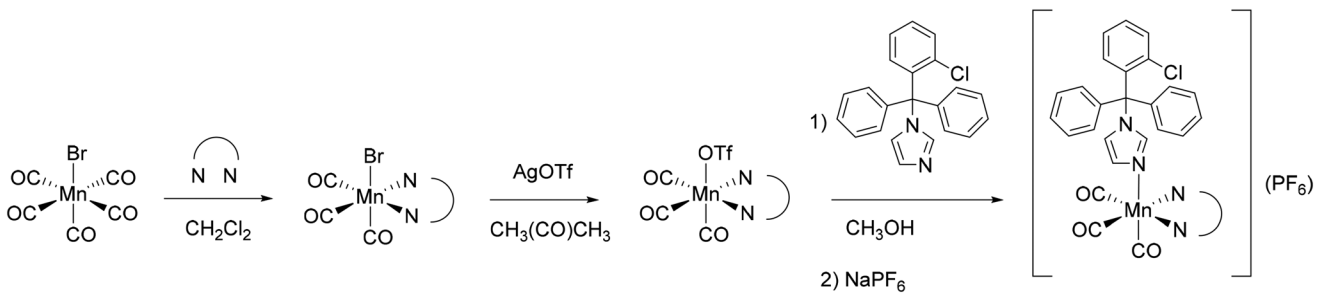

Fig. 2 Synthesis scheme of the *fac*-$[Mn(CO)_3(CTZ)(NN)](PF_6)$ compounds.

Synthesis of the *fac*-[MnBr(CO)$_3$(NN)] precursors

The *fac*-[MnBr(CO)$_3$(NN)] precursors were obtained through modifications of literature procedures by reaction of equimolar amounts of [MnBr(CO)$_5$] and the corresponding NN ligands in CH_2Cl_2. Elemental analyses, FTIR and NMR results agreed with those previously reported for NN = phen, bipy, dmb and aminophen, while a novel precursor, *fac*-[MnBr(CO)$_3$(tmp)], is reported in this work.[62]

Synthesis of the new precursor *fac*-[MnBr(CO)$_3$(tmp)]

MnBr(CO)$_5$ (100.0 mg, 0.364 mmol) and tmp (86.0 mg, 0.364 mmol) were suspended in 6 mL of CH_2Cl_2. The yellow suspension was stirred at room temperature for 24 h. A pale-yellow solid was obtained, washed twice with 2 mL of CH_2Cl_2, and dried under vacuum. Yield: 147.4 mg (0.324 mmol), 89%. Anal. calc. for $C_{19}H_{16}BrMnN_2O_3$: C, 50.13; H, 3.54; N, 6.15%. Found: C, 50.07; H, 3.42; N, 6.15%. FTIR (KBr, cm^{-1}): 2026, 1934, 1912 (vs) ν(C≡O), 1616, 1525, 1428, 1384 (m) ν(C=N), (C=C), (C–N), (C–C), 822, 728, 682, 633 (s) δ(C–H). ^{1}H-NMR (400 MHz, DMSO-d$_6$), δ (ppm): 9.28 (2H, s, H19), 8.38 (2H, s, H24, H25), 2.81 (6H, s, H22, H23), 2.64 (6H, s, H20, H21).

Synthesis of the *fac*-[Mn(CO)$_3$(CTZ)(NN)](PF$_6$) final compounds

The *fac*-[Mn(CO)$_3$(CTZ)(NN)](PF$_6$) compounds were obtained through a modification of literature procedures by reaction of equimolar amounts of silver triflate (AgOTf) and the corresponding *fac*-[MnBr(CO)$_3$(NN)] (0.220–0.255 mmol) precursors in 6 mL of acetone for 3 h at room temperature. Generated silver bromide was removed, and the solvent of the supernatant was evaporated by vacuum. The obtained *fac*-[Mn(OTf)(CO)$_3$(NN)] was redissolved in 5 mL of MeOH and an equimolar amount of CTZ (considering a yield of 100%, 0.220–0.250 mmol) was added and stirred for 24 h at room temperature. The hexafluorophosphate salt was precipitated by addition of twice the equimolar amount of $NaPF_6$ (0.440–0.510 mmol) and stirring for 24 h at room temperature. The obtained solids were separated by centrifugation and washed twice with 2 mL of a MeOH : H_2O 1 : 1 mixture. Quantities of reagents in each synthetic procedure are detailed below for each compound. Elemental analysis, FTIR and NMR results of *fac*-[Mn(CO)$_3$(CTZ)(bipy)](PF$_6$) compound obtained agreed with those previously reported by Simpson *et al.*; meanwhile for the other NN ligands, the compounds obtained were novel and consistent with the proposed formula.

fac-[Mn(CO)$_3$(CTZ)(phen)](PF$_6$)

fac-[MnBr(CO)$_3$(phen)] (100.0 mg, 0.251 mmol), AgOTf (64.4 mg, 0.251 mmol), CTZ (86.4 mg, 0.251 mmol), $NaPF_6$ (84.1 mg, 0.501 mmol). A bright yellow solid was obtained. Yield: 156.1 mg (0.193 mmol) 77%. Anal. calc. for $C_{37}H_{25}ClF_6MnN_4O_3P$: C, 54.93; H, 3.12; N, 6.93%. Found: C, 54.65; H, 3.05; N, 6.96%. FTIR (KBr, cm^{-1}): 2042, 1957, 1933 (vs) ν(C≡O), 1446, 1431 (m) ν(C=N), (C=C), (C–N), (C–C), 857 (s) δ(C–H), 840 (vs) ν(P–F), 766, 752, 726, δ(C–H), 557 δ(P–F). ^{1}H-NMR (400 MHz, DMSO-d$_6$), δ (ppm): 9.61 (2H, dd, J = 5.05, 1.25 Hz, H18), 8.88 (2H, dd, J = 8.24, 1.29 Hz, H20), 8.27 (2H, s, H21), 8.04 (2H, dd, J = 8.21, 5.05 Hz, H19), 7.41 (1H, td, J = 7.64, 1.59 Hz, H15), 7.32 (2H, m, H6, H11), 7.23 (6H, m, H5, H7, H10, H12, H16), 7.02 (1H, t, J = 1.56 Hz, H1), 6.87 (1H, t, J = 1.70 Hz, H2), 6.54 (5H, m, H4, H8, H9, H13, H14), 6.32 (1H, t, J = 1.52 Hz, H3). ^{31}P{^{1}H}-NMR (162 MHz, DMSO-d$_6$), δ (ppm): −145.09 (sept, J = 711.37 Hz, PF_6).

fac-[Mn(CO)$_3$(CTZ)(dmb)](PF$_6$)

fac-[MnBr(CO)$_3$(dmb)] (100.0 mg, 0.248 mmol), AgOTf (63.7 mg, 0.248 mmol), CTZ (85.5 mg, 0.248 mmol), $NaPF_6$ (83.3 mg, 0.496 mmol). A bright yellow solid was obtained. Yield: 149.2 mg (0.184 mmol) 74%. Anal. calc. for $C_{37}H_{29}ClF_6MnN_4O_3P$: C, 54.66; H, 3.60; N, 6.89%. Found: C, 54.61; H, 3.67; N, 6.88%. FTIR (KBr, cm^{-1}): 2040, 1946, 1937 (vs) ν(C≡O), 1617, 1491, 1448 (m) ν(C=N), (C=C), (C–N), (C–C), 910, 858 (m) δ(C–H), 840 (vs) ν(P–F), 762, 708, 635 (s) δ(C–H), 557 (s) δ(P–F). ^{1}H-NMR (400 MHz, DMSO-d$_6$), δ (ppm): 9.01 (2H, d, J = 5.65 Hz, H18), 8.45 (2H, s, H21), 7.53 (2H, d, J = 5.76 Hz, H19), 7.48 (1H, td, J = 7.63, 1.60 Hz, H15), 7.41–7.31 (8H, m, H5, H6, H7, H10, H11, H12, H16, H17), 7.01 (1H, t, J = 1.51 Hz, H1), 7.00 (1H, t, J = 1.60 Hz, H2), 6.73 (4H, H4, H8, H9, H13), 6.68 (1H, dd, J = 8.00, 1.58 Hz, H14), 6.47 (1H, t, J = 1.55 Hz, H3), 2.51 (6H, s, H20). ^{31}P{^{1}H}-NMR (162 MHz, DMSO-d$_6$), δ (ppm): −144.98 (sept, J = 711.35, PF_6).

fac-[Mn(CO)$_3$(CTZ)(tmp)](PF$_6$)

fac-[MnBr(CO)$_3$(tmp)] (100.0 mg, 0.220 mmol), AgOTf (56.4 mg, 0.220 mmol), CTZ (75.7 mg, 0.220 mmol), $NaPF_6$ (73.8 mg, 0.439 mmol). A pale-yellow solid was obtained. Yield: 163.4 mg (0.189 mmol) 86%. Anal. calc. for $C_{41}H_{33}ClF_6MnN_4O_3P$: C, 56.92; H, 3.85; N, 6.48%. Found: C, 56.75; H, 3.88; N, 6.52%. FTIR (KBr, cm^{-1}): 2037, 1956, 1920 (vs) ν(C≡O), 1528, 1446, 1431 (m) ν(C=N), (C=C), (C–N), (C–C), 873 (s) δ(C–H), 840 (vs) ν(P–F), 752, 709, 638 (s) δ(C–H), 557 (s) δ(P–F). ^{1}H-NMR (400 MHz, DMSO-d$_6$), δ (ppm): 9.32 (2H, s, H19), 8.34 (2H, s, H24, H25), 7.43 (1H, t, J = 7.68 Hz, H15), 7.34 (2H, t, J = 7.34 Hz, H6, H11), 7.25 (5H, m, H5, H7, H10, H12, H16), 7.14 (2H, m, H1, H17), 6.89 (1H, brs, H2), 6.61 (1H, d, J = 8.10 Hz, H14), 6.56 (4H, d, J = 7.82 Hz, H4, H8, H9, H13), 6.42 (1H, brs, H3), 2.78 (6H, s, H22, H23), 2.56 (6H, s, H20, H21). ^{31}P{^{1}H}-NMR (162 MHz, DMSO-d$_6$), δ (ppm): −145.31 (sept, J = 711.21, PF_6).

fac-[Mn(CO)$_3$(CTZ)(aminophen)](PF$_6$)

fac-[MnBr(CO)$_3$(aminophen)] (100.0 mg, 0.241 mmol), AgOTf (62.0 mg, 0.241 mmol), CTZ (83.3 mg, 0.241 mmol), $NaPF_6$ (81.1 mg, 0.483 mmol). An orange solid was obtained. Yield: 107.4 mg (0.130 mmol) 54%. Anal. calc. for $C_{37}H_{26}ClF_6MnN_5O_3P$: C, 53.93; H, 3.18; N, 8.50%. Found: C, 53.72; H, 3.24; N, 8.55%. FTIR (KBr, cm^{-1}): 3508, 3416 (m) ν(N–H), 2037, 1951, 1930, 1912 (vs) ν(C≡O), 1638, 1598, 1495, 1468, 1433 (m) ν(C=N), (C=C), (C–N), (C–C), 842 (vs) ν(P–F), 753, 729, 711, 634 (m) δ(C–H), 557 (s) δ(P–F). ^{1}H-RMN (400 MHz, DMSO-d$_6$), δ (ppm): 9.54 (1H, d, J = 5.00 Hz, H19), 9.08 (1H, d, J = 4.91 Hz, H18), 9.01 (1H, d, J = 8.49 Hz, H23), 8.38 (1H, d, J = 8.35 Hz, H22), 7.98 (1H, dd, J = 8.46, 5.08 Hz,

H21), 7.72 (1H, dd, J = 8.33, 4.96 Hz, H20), 7.43 (1H, t, J = 7.67 Hz, H15), 7.33 (2H, m, H6, H11), 7.25 (6H, m, H5, H7, H10, H12, H16, H17), 7.02 (1H, t, J = 1.50 Hz, H1), 6.96 (1H, s, H24), 6.89 (3H, m, H2, H25, H26), 6.53 (5H, m, H4, H8, H9, H13, H14), 6.21 (1H, t, J = 1.55 Hz, H3). $^{31}P\{^1H\}$-NMR (162 MHz, DMSO-d_6), δ (ppm): −145.61 (sept, J = 711.31, PF_6).

Biological studies

In vitro activity against *T. cruzi*, *L. infantum* and cytotoxicity on VERO cells as mammalian cell model

Parasites and cell culture. T. cruzi epimastigotes Dm28c and *L. infantum* promastigotes were maintained at 28 °C in brain–heart infusion medium (BHI) supplemented with 10% fetal bovine serum (heat inactivated, FBS), penicillin (100 units per mL) and streptomycin (100 μg mL^{-1}), and were harvested during the exponential phase of growth.[28,29]

VERO cells (ATCC CCL81) were used as the mammalian cell model for the evaluation of the unspecific cytotoxicity and as host cell for *T. cruzi* trypomastigotes infection. Cells were cultured at 37 °C in RPMI-1640 medium supplemented with 10% FBS, penicillin (100 units per mL) and streptomycin (100 μg mL^{-1}) in a humidified 5% CO_2 incubator. For maintenance, confluent cells were washed with PBS, incubated for 3 min with trypsin–EDTA and diluted.[63]

T. cruzi infections were established incubating a monolayer of VERO cells with metacyclic trypomastigotes, differentiated by nutritional stress, in a 10 : 1 parasite : cell ratio at 37 °C in RPMI medium in a humidified 5% CO_2 incubator. The remaining parasites were removed 24 h later by aspirating and washing the infected cells with PBS. The emerging trypomastigotes (4–5 days post-infection) were used to establish a new VERO cell infection.[64]

Cell-derived trypomastigotes used in the evaluation experiments were obtained from the supernatant of infected VERO cells 24 h after the trypomastigotes began emerging, following a wash with PBS.[64]

In vitro activity against epimastigotes and trypomastigotes of T. cruzi, and promastigotes of L. infantum. An amount of 1×10^6 parasites per well was seeded in a 96-well black plate, using BHI for *T. cruzi* epimastigotes and *L. infantum* promastigotes or RPMI for *T. cruzi* trypomastigotes, and treated with increasing concentrations of the compounds for 24 h at 28 °C (*T. cruzi* epimastigotes and *L. infantum* promastigotes) or 37 °C (*T. cruzi* trypomastigotes). The compounds were initially dissolved in DMSO and further diluted in culture medium to obtain the different concentrations tested. In *T. cruzi* experiments, the concentration of DMSO did not exceed 1%, which is non-toxic for the parasites.[65]

Particularly for *L. infantum* experiments, the amount of DMSO was normalized to 1% per well, as fluorescence quenching was observed at lower concentrations.

To measure the metabolic activity of the parasites after incubation, 50 μL of resazurin solution (2 mg mL^{-1} for *T. cruzi* or 2.5 mg mL^{-1} for *L. infantum*) was added to each well and incubated for additional 4 h, protected from light. Fluorescence (λ_{ex} 530 nm/λ_{em} 590 nm) was measured using a Thermo Scientific Varioskan® fluorimeter. The EC_{50} at 24 h was determined from sigmoidal dose–response curves using GraphPad Prism version 8.00 for Windows. Results are expressed as mean values ± standard deviation (SD) from three independent biological replicates. Nifurtimox was used as the reference drug against *T. cruzi*.[28,29,64]

Unspecific cytotoxicity on VERO cells. The MTT reduction assay was used to assess the cytotoxicity of the compounds on VERO cells as a mammalian cell model.[66]

A total of 1000 cells per well were seeded in 96-well plates and incubated at 37 °C with 5% CO_2 for 24 h to allow cell adherence. Increasing concentrations of each compound were added and incubated for additional 24 h. For the viability assay, 20 μL of MTT solution (5 mg mL^{-1} in PBS) were added, and the plates were incubated for 4 h at 37 °C. The medium was then aspirated, and the cells were lysed using DMSO. Absorbance at 570 nm was measured using a Thermo Scientific Varioskan Flash Multimode spectrophotometer, and the EC_{50} values were determined from the fitted dose–response curve. The obtained EC_{50} values are presented as mean ± standard deviation of three independent biological replicates.

Stability in solution

The chemical stability of the final compounds *fac*-$[Mn(CO)_3(CTZ)(NN)](PF_6)$ was studied in the following media: DMSO, DMSO : BHI-tryptose (10% FBS) (50 : 50) and DMSO : FBS (50 : 50), employing reverse phase high-performance liquid chromatography (RP-HPLC-DAD).[67]

BHI is the culture medium in which the parasites are grown for biological assays; meanwhile FBS was used as a model of the behaviour in human serum. A Shimadzu Prominence LC-20AT liquid chromatograph was used, coupled to a Shimadzu PD-M20A diode array detector. An Agilent ZORBAX Eclipse Plus C18 column (4.6 × 100 mm; 3.6 μm), thermostated at 25 °C, was used as the stationary phase. A 40 mM phosphate buffer solution pH 7.4 (A) and MeOH (B) were used as mobile phases flowing at a constant flow rate of 1 mL min^{-1}, according to the gradient shown in Table S1.† [67,68]

For the preparation of the solutions, 1 mg of each compound was dissolved in 2.0 mL of each medium. The obtained solutions were filtered using 0.45 μm pore size PVDF transfer membranes. An injection volume of 50 μL was established per run. The monitoring wavelength was 250 nm. Stability was studied over a period of 5 days for DMSO, the solutions being measured at t = 0 h, t = 24 h and t = 120 h under the same chromatographic conditions. Similarly, the stability in DMSO : supplemented BHI medium (50 : 50) and DMSO : FBS (50 : 50) was studied over a period of 1 day, the being solutions measured at t = 0 h and t = 24 h.

Lipophilicity studies

Experimental determination. The lipophilicity of the final compounds, *fac*-$[Mn(CO)_3(NN)(CTZ)](PF_6)$, was studied in solution by RP-HPLC-DAD.[69,70] A Shimadzu Prominence LC-20AT liquid chromatograph coupled to a Shimadzu PD-M20A diode

array detector was used. An Agilent ZORBAX Eclipse Plus C8 (4.6 × 250 mm, 5.0 μm) was employed as the stationary phase. A mixture of MeOH : 40 mM phosphate buffer pH 7.4 (70 : 30) was used as the mobile phase, flowing at a constant rate of 0.8 mL min^{-1} in isocratic mode. The injection volume was 50 μL. The monitoring wavelength was 250 nm. Solutions were prepared by dissolving 1 mg of each compound in 2 mL DMSO and were filtered using 0.45 μm pore size PVDF transfer membranes. Tartrazine was used for the estimation of the hold-up time (t_0). This compound is often used to estimate t_0 of a chromatographic column, because of its low affinity for nonpolar stationary phases—such as C8—given its polar properties.[71]

Computational insights into lipophilicity of analogous Re and Mn final compounds. An initial screening of functionals and basis sets was conducted to identify the most suitable level of theory for calculating water–octanol partition coefficients (log *P*) that best align with experimental evidence for the Re(I) tricarbonyl complexes.[29,72]

Specifically, combinations of six functionals and four basis sets were tested on *fac*-[$Re(CO)_3$(CTZ)(phen)](PF_6) complex, whose crystalline structure and experimental log *P* were known, employing the SMD solvation model. The log *P* values were derived from the Gibbs free energy change (ΔG) associated with solvent transfer, as previously described in the literature.[72,73]

This analysis identified LANL2DZ as the most suitable basis set, paired with four high-performing functionals: B3LYP, M06L, ωB97XD, and PBE0. These combinations were then employed to calculate the log *P* values for the rest of the Re(I) complexes. Based on these results, the two top-performing combinations—M06L/LANL2DZ and ωB97XD/LANL2DZ—were subsequently applied to the Mn(I) tricarbonyl complexes. The SMD implicit solvation model was consistently applied, with enhancements for aminophen-containing complexes, where two explicit water molecules were added to model hydrogen bonding with the –NH_2 substituent. Additional details regarding the computational strategy are provided in the ESI.†

Insight into the mechanism of action

DNA interaction studies by fluorescence quenching studies. A DNA stock solution was prepared by hydrating ctDNA (calf thymus DNA, Sigma, type I, no. D-1501) in 10 mM Tris-HCl buffer (1 mg mL^{-1}, ~2 mM nuc^{-1}), and was allowed to stand 48 h at 4 °C. The concentration of the stock solution was determined by UV spectrophotometry using the molar absorption coefficient ε (260 nm) = 6600 M^{-1} cm^{-1} nuc^{-1}.[28]

Competitive binding assays between ethidium bromide (EB, Sigma) and organometallic Mn compounds were conducted in a 10 mM Tris-HCl buffer at pH 7.4. Fluorescence measurements were performed using a fixed concentration of ctDNA and EB, while the concentration of the Mn complexes was progressively increased.

An EB 0.5 mM solution was prepared in Tris-HCl buffer. To improve the solubility of the complexes in aqueous media, DMSO was used to prepare concentrated stock solutions, followed by appropriate dilution. The final samples contained no more than 5% v/v DMSO. Samples were prepared with a total concentration of DNA and EB of 20 μM and 10 μM, respectively, and the concentration of the Mn compounds was varied between 0 and 60 μM. Following incubation at 37 °C for 30 min, fluorescence spectra were recorded from 540 to 680 nm at an excitation wavelength of 510 nm on a Shimadzu RF5310 spectrofluorometer. Control samples containing only the compounds and ctDNA (excluding EB) were used as blanks, and their spectra were subtracted from the experimental data. The Stern–Volmer equation (eqn (1)) was applied to calculate the quenching constants and evaluate the binding competition.[74]

$$IF_0/IF = 1 + K_{SV}[Q] = 1 + k_q\tau[Q] \quad (1)$$

IF_0 and IF are the fluorescence intensity of the {DNA : EB} adduct in the absence and presence of the compounds, respectively. K_{SV} is the Stern–Volmer quenching constant, k_q is the bimolecular quenching rate constant, [Q] is the concentration of the quencher, and τ is the average lifetime of the biomolecule in the excited state (typically *ca.* 10^{-8} s for biomacromolecules).[75,76] K_{SV} values were obtained from the plot of IF_0/IF *vs.* [Q].

Inhibition of the biosynthesis of membrane sterols

The study was performed on *Trypanosoma cruzi* (Dm28c) epimastigotes and *Leishmania infantum* promastigotes at a density of 1 × 10^7 parasites per mL. The most promising compound *fac*-[$Mn(CO)_3$(CTZ)(tmp)](PF_6) was dissolved in DMSO and applied at concentrations of 0.8 μM and 4.0 μM, equivalent to 1× and 5× the EC_{50} values obtained from *in vitro* assays for *T. cruzi* and *L. infantum*. Parasites were incubated with the compound for 4 h at 28 °C. Untreated parasites served as a negative control, and the DMSO concentration in the culture medium was maintained below 0.4% v/v.[29,77,78]

After incubation, sterols (ergosterol, lanosterol, and squalene) were extracted from the parasite. The samples were first centrifuged at 3000 rpm for 10 min, and the supernatants were discarded. The resulting pellets were resuspended in 1 mL of phosphate buffer (0.05 M, pH 7.4) and centrifuged again at 3000 rpm for 10 min, followed by discarding the supernatants. The pellets were resuspended in 1 mL of a $CHCl_3$: MeOH (2 : 1) solution and stored at 4 °C for 12 h. Subsequently, 2 mL of saturated NaCl solution was added, and the mixture was extracted with 1 mL of $CHCl_3$, carefully avoiding the aqueous phase. This extraction step was repeated twice to ensure complete recovery of the sterols.[29,77,78]

The collected organic phase was evaporated under nitrogen and redissolved in 1 mL of acetonitrile for analysis by high-performance liquid chromatography coupled with diode array detection (HPLC-DAD). The chromatographic system utilized a C8 stationary phase (250 × 4.6 mm, 5 μm), with acetonitrile as the mobile phase at a flow rate of 0.9 mL min^{-1}. Detection was carried out at a wavelength of 210 nm.[78]

CO release assays

All assays were carried out under controlled light exposure. The CO photoinduced release was investigated by IR and UV-

vis spectroscopy. For the application of electromagnetic radiation, a system containing a quartz cuvette (for UV-vis) or CaF_2 (for IR) filled with the sample was inserted in a box in which the exposure time to light was computationally controlled using the Arduino 1.8.15 IDE and an Arduino UNO R3 board.

The light source employed to perform the CO release assays was one set with four LEDs in series, with the wavelength 395 ± 10 nm. The distance between the cuvette and the LEDs were set to 3 cm, and the light source was arranged perpendicularly to the sample.

The CO release for the compounds was verified by monitoring the variation in the electronic spectra (200–500 nm) and in the carbonyl stretching region (2250–1750 cm^{-1}).[56,79]

UV-vis. The compounds were dissolved in CH_2Cl_2 at 1 mM, and further diluted so that the initial absorbance of the MLCT band was between 0.2 and 0.3, and the solution was irradiated. Spectra were acquired between 200–900 nm.

IR. The compounds were dissolved in CH_2Cl_2 at 1 mM and the solution was irradiated. Spectra were acquired between 2250–1750 cm^{-1}.

Additionally, CO release of the Mn compounds in aqueous medium in the dark was tested by incubation of the compounds at 0.5 mM in DMSO : buffer phosphate 40 mM pH 7.4 (50 : 50). UV-vis spectra were acquired between 300 and 900 nm over a period of 24 h.

Metallomics

T. cruzi Dm28c epimastigotes were treated with the most promising compound, *fac*-[Mn(CO)$_3$(CTZ)(tmp)](PF$_6$), and its uptake and distribution in the parasite was studied.

Uptake. Parasites at a density of 6×10^6 parasites per mL were cultured in BHI medium at 28 °C and incubated with concentrations of *fac*-[Mn(CO)$_3$(CTZ)(tmp)](PF$_6$) at concentrations corresponding to 1× EC_{50} and 10× EC_{50} previously determined on *T. cruzi* epimastigotes. Parasites were collected at 4 and 24 h of incubation by centrifugation at 1000*g* for 10 min. The supernatant containing uncaptured compound was separated from the pellet of parasites. The pellet was washed with phosphate buffered saline solution (PBS) and resuspended in 500 µL of 0.1 M HNO_3 and subjected to ultrasonication for 5 min in a Cole Parmer 8893 ultrasonic bath at 47 kHz for optimum solubilization. The supernatant was appropriately diluted with 0.1 M HNO_3. The two fractions obtained, supernatant and pellet, were analysed by electrothermal atomic absorption spectrometry (ET-AAS) employing a Thermo Scientific iCE 3500 spectrometer with Zeeman correction. The uptake of manganese in the parasites was determined with the following equation, where "pellet" corresponds to the total µg of manganese in the pellet and "supernatant" to the total µg of manganese in the supernatant:

$$\%\,\text{uptake} = \frac{\text{pellet} \times 100}{(\text{pellet} + \text{supernatant})} \quad (2)$$

Three independent experiments were carried out for each concentration at each studied time point.[33]

Association with macromolecules. Manganese association with different subcellular fractions (soluble proteins, DNA, RNA and insoluble fraction) was studied for *fac*-[Mn(CO)$_3$(CTZ)(tmp)](PF$_6$) as previously described.[64]

After 4 h of incubation, the different biomacromolecules were isolated for further analysis. For isolating DNA, parasites were collected using Monarch genomic DNA purification kit provided by New England Biolabs (Ipswich, MA, USA). For isolating proteins, parasites were resuspended in 1 mL of parasite lysis buffer containing Tris-HCl 10 mM pH = 7.5, EDTA 1 mM, CHAPS 1%, glycerol 10%, Triton 0.5% and Complete™ protease inhibitor cocktail provided by Roche (Manheim, Germany). After stirring on ice for 30 min, the lysate was centrifugated at 20 000*g* for 1 h at 4 °C. The soluble proteins were isolated from the supernatant and the insoluble ones from the pellet, which were resuspended in 200 µL of PBS. The insoluble fraction contained mostly insoluble proteins and membrane lipids, among other insoluble molecules. For isolating total RNA a Trizol™ reagent provided by Life Technologies (Gaithersburg, MD, USA) was used. All fractions were diluted to 500 µL with 0.1 M HNO_3 and subjected to ultrasonication for 5 min in the ultrasonic bath at 47 kHz for optimum solubilization. Three independent experiments were carried out for each fraction at each concentration.

The samples were analyzed by ET-AAS. Associated percentages were calculated as following, where "*x*" was a given biomacromolecule fraction, and "total µg of Mn" was the sum of Mn in all the studied fractions (DNA fraction, RNA fraction, soluble proteins and insoluble fraction):

$$\%\,\text{Mn fraction } x = \frac{\mu\text{g of Mn in fraction } x \times 100}{\text{total } \mu\text{g of Mn}} \quad (3)$$

Confocal Raman microscopy

Parasites were exposed to *fac*-[Mn(CO)$_3$(CTZ)(tmp)](PF$_6$) at concentrations equivalent to 1×, 5× and 10× the EC_{50} value for durations of 4 h. Following treatment, the samples were placed onto a silicon substrate and dried using a nitrogen stream. Control parasites, left untreated, were analyzed under the same conditions for comparison.

Confocal Raman imaging analysis was conducted using a WITec Confocal Raman Microscopy Alpha 300 RA system. A 532 nm excitation laser wavelength was employed with intensity adjusted to prevent cell damage. Images were captured within a scan area of approximately 6 µm × 6 µm, using a grid of 40 points per line and 40 lines per image. Each spectrum was recorded with an acquisition time of 0.5 seconds.

Proteomics

Parasite culture and incubation with compounds for proteomics studies. Three independent cultures of epimastigotes of *Trypanosoma cruzi* at a density of 1×10^7 epimastigotes per mL were treated with 1× EC_{50} of *fac*-[Mn(CO)$_3$(CTZ)(tmp)](PF$_6$) (0.81 µM) and *fac*-[Re(CO)$_3$(CTZ)(tmp)](PF$_6$) (3.48 µM) during 4 h. Untreated parasites were also cultured as a control. After

the incubation, parasites were centrifuged for 10 min at 3000 rpm, washed twice with PBS and the parasite pellet was kept at −20 °C.[80]

Protein extraction and quantification. For total protein isolation, treated and control parasites were centrifugated, incubated with lysis buffer (7 M urea, 2 M thiourea, 4% CHAPS) at 4 °C for 30 min and finally centrifuged at 4 °C at 20 000*g* for 1 h to separate soluble and insoluble fraction. The protein fraction was further processed for the proteomic analysis.[80]

Protein sample processing for nano-LC-MS/MS analysis. Total protein from epimastigotes of *Trypanosoma cruzi* Dm28c untreated, treated with *fac*-[$Mn(CO)_3$(CTZ)(tmp)](PF_6) and with *fac*-[$Re(CO)_3$(CTZ)(tmp)](PF_6) were subjected to protein identification by LC-MS/MS analysis using three independent biological replicates per condition. Samples were prepared using the eFASP (enhanced filter-aided sample preparation) protocol with slight modifications.[81]

Amicom Ultra 0.5 mL centrifugal filters (10 kDA MWCO) were pretreated with 5% Tween20 for 3 h at room temperature with gentle agitation, and then thoroughly washed with ultrapure water. The working buffer consisted of 4 M urea, 40 mM Tris·Cl, pH 7.5.

A total of 100 μg of proteins for each sample was diluted in the working buffer and loaded into eFASP ultrafiltration (UF) units. Samples were reduced with 10 mM DTT and subsequently alkylated with 50 mM iodoacetamide. Both reagents were prepared in the working solution and the reactions were performed at room temperature for 1 h. Each buffer exchange step was carried out by centrifugation at 14 000*g* for 15 min at room temperature.

Protein digestion was performed in eFASP UF units using 0.1 mg mL^{-1} sequence grade trypsin (Promega) in 50 mM ammonium bicarbonate pH 8.0, incubation overnight at 37 °C. For peptide recovery, eFASP UF units were transferred to new collection tubes and centrifuged at 14 000*g* for 15 min, followed by two washes with 0.1% formic acid. The resulting peptide samples were then vacuum concentrated and desalted using C18 micro-columns (C18 OMIX pipette tips, Agilent). Finally, peptide samples were resuspended in 0.1% formic acid and peptide concentrations were measured in a DeNovix DS-11 FX+ spectrophotometer/fluorometer at 215 nm.

NanoLC-MS/MS analysis. A shotgun proteomic strategy was used to compare the protein profiles of untreated parasites and treated with the two different compounds under study (*fac*-[$Mn(CO)_3$(CTZ)(tmp)](PF_6) and *fac*-[$Re(CO)_3$(CTZ)(tmp)](PF_6)). For this purpose, a nano-HPLC Ultimate 3000 system (Thermo Scientific) coupled online to an OrbitrapExploris 240 (Thermo Scientific) mass spectrometer through an Easy-Spray source was used. 5 μg of tryptic peptides were injected into an Acclaim PepMap™100 C18 nano-trap column (75 μm × 2 cm, 3 μm particle size), and separated using a 75 μm × 50 cm, Easy-Spray™ analytical C18 HPLC column (2 μm particle size, 100 Å pore size) at a constant flow rate of 200 nL min^{-1} and 40 °C and applying the following gradient: from 5% to 35% mobile phase B (0.1% formic acid in acetonitrile) over 150 min, followed by 35% to 99% mobile phase B over 15 min. Three independent biological replicates and two technical replicates per sample were analyzed. All nano-LC-MS/MS equipment and supplies were from Thermo Scientific. The mass spectrometer was operated in the positive mode. The ion spray voltage was set at 2.2 kV, the capillary temperature at 250 °C, and the S-lens RF level at 50. Mass analysis was conducted in data-dependent mode in two steps. First, full MS scans were acquired in a *m*/*z* range from 200 to 2000, with a resolution of 90 000 ppm. This was followed by HCD fragmentation of the 20 most intense ions in each duty cycle, using stepped normalized collision energy of 25, 30 and 35, and a resolution of 25 000 ppm. Precursor ions with charge states ranging from 2 to 5 were included for fragmentation. The dynamic exclusion was set after $n = 2$ detections within 30 s, with an exclusion duration of 10 s.

Proteomic data analysis

Database generation, protein identification, and subsequent analyses were conducted using the PatternLab V software (**https://www.patternlabforproteomics.org**).[82]

For that purpose, protein sequences from *Trypanosoma cruzi* Dm28c strain were obtained from Uniprot Consortium (in December, 2023) (**https://www.uniprot.org**) and protein sequences of the 127 most prevalent mass spectrometry contaminants were included to generate a target-decoy database. Raw files were searched against the database using the Comet search engine applying the following parameters: fully specific trypsin as proteolytic enzyme allowing up to 2 missed cleavages; methionine oxidation as variable modification, cysteine carbamidomethylation as fixed modification; and a precursor mass tolerance of 40 ppm. Peptide spectrum matches were filtered using the Search Engine Processor (SEPro), using stringent FDR criteria set at 3% at spectrum level, 2% at peptide level, and 1% at the protein level. To identify proteins exclusively detected in each sample set, PatternLab's approximately area-proportional Venn diagram module was used with a significant threshold of p-value ≤0.05. For detecting proteins present in both conditions but showing significantly different relative abundances, the pairwise comparison module was used by means of extracted ion chromatogram (XIC) analysis, applying the following statistical criteria: log2 fold change ≤1, and p-value ≤0.05. Overrepresentation of GO terms among differentially expressed protein lists was established using the available tool at TritrypDBdatabase (**https://tritrypdb.org/tritrypdb/app/**) setting a Bonferroni adjusted p-value ≤0.5 as a cutoff for significance.

Results and discussion

The five proposed compounds were synthesized through a four-stepped procedure with high purities and acceptable yields (Fig. 2). In the first step, two carbonyl ligands of [$MnBr(CO)_5$] were substituted by the bidentate NN ligand by stirring the mixture in CH_2Cl_2, leading to the five *fac*-[$MnBr(CO)_3$(NN)] precursors. Then, adding silver triflate (AgOTf) and stirring the mixture in acetone led to the substitution of bromide by

triflate promoted by the precipitation of insoluble AgBr. The solutions of *fac*-[Mn(OTf)(CO)$_3$(NN)] were stirred with CTZ in MeOH, resulting in the substitution of the triflate ligand. The final compounds were precipitated as the hexafluorophosphate salts. One of the precursors, *fac*-[MnBr(CO)$_3$(tmp)], as well as four of the final compounds, *fac*-[Mn(CO)$_3$(CTZ)(NN)](PF$_6$) where NN = phen, dmb, tmp, aminophen, are novel.

The obtained compounds were slightly soluble in organic hydrophilic solvents, like MeOH or EtOH, moderately soluble in DMSO and practically insoluble in water.

Although the synthetic strategy was similar to that developed by our research group for the synthesis of the analogous Re compounds, those experimental conditions, such as solvent type and reaction temperature, did not lead to the desired manganese analogues.[29] One possible reason for this behaviour, particularly in respect to the temperature, is the fact that manganese is a 3d transition metal, while rhenium is 5d, which implies that more drastic conditions are needed for rhenium to react when compared with manganese. Too drastic synthetic conditions led to decomposition for manganese(I) compounds, meanwhile mild reaction conditions resulted in the desired products.

All the final compounds were fully characterized in solid state and in solution by elemental analysis, conductometric measurements and UV-Vis, FTIR and NMR (^{1}H, ^{31}P) spectroscopy.

Characterization of the compounds in the solid state

The elemental analyses of the final compounds were in accordance with the calculated data for the proposed formula. Due to refractory behaviour of the rhenium analogues, we needed to use V_2O_5 as a catalyst to allow complete decomposition of the sample and accurate analysis, but this modification of the classical method was not needed for the manganese compounds.[33]

The FTIR spectra showed characteristic vibration bands of the structural units of the manganese compounds—tricarbonyl centre, bioactive ligands and counterion. In general, the vibrational bands of the ligands shifted when compared with the free ligands. In all cases there were bands in the 2050–1900 cm^{-1} region in a three-band pattern typical of the stretching of the tricarbonyl centres ν(C≡O); in the 1650–1300 cm^{-1} region, typical of the stretch of C=N and C=C bonds of the CTZ and NN ligands; and for the final compounds, bands at 840 and 557 cm^{-1}, characteristic of the PF_6^- counterion (Fig. S1–S6†).[42,56,60,79,83,84]

Characterization of the compounds in solution

Conductivity measurements. Conductivity of 10^{-3} M DMSO solutions was measured to evaluate the electrolyte stoichiometry. Obtained molar conductivity values were in the characteristic range for 1 : 1 electrolytes (28–34 S cm^2 mol^{-1}), which is in accordance with the proposed formula. No significant variations were observed in conductivity for 5 days.[85]

^{1}H and ^{31}P-NMR results. Fig. S7† shows the numbering scheme of the ligands in all the metal compounds. ^{1}H-NMR spectra and COSY correlation NMR experiments, as well as ^{31}P-NMR spectra were recorded in DMSO-d$_6$ solution to completely characterize the obtained compounds. All the complexes showed a pattern of signals corresponding to the protons of CTZ and the NN ligands. Integration and multiplicities of the signals were in accordance with the proposed formula of the compounds (Fig. S8–S23†).

In the region of 9.7–6.2 ppm, signals of the protons of CTZ and the aromatic protons of the NN derivatives were observed and assigned. For NN = dmb and tmp, signals of the methyl groups were also observed at 2.9–2.4 ppm. Due to the coordination to the organometallic centre, most of the signals shifted when compared with the free ligands. Particularly, all signals of NN ligands shifted to lower fields, indicating a decrease in electronic density; meanwhile for the Clotrimazole, the shifts were to lower and higher fields, depending on the position of the proton, showing a redistribution of electronic density in the ligand when coordinated. The signals of the protons adjacent to the coordination site in CTZ, H1 and H2, were the most affected.

In the ^{31}P-NMR spectra, the characteristic septuplet of the PF_6^- counterion was evidenced in all cases.

When comparing the ^{1}H-NMR spectra of the Mn(I) final compounds with their Re(I) analogues, a significant resemblance was observed. The general behaviour of the signals of each ligand when coordinating was the same for both organometallic centres. Small differences among the chemical shifts of the signals were noticed and assigned to the differential capacity of attracting and delocalizing electrons of each centre. For H1 and H2 protons, adjacent to the coordination site in CTZ ligand, the difference in the chemical shifts between Mn (I) and Re(I) compounds was the highest.

Biological studies

Anti-*Trypanosoma cruzi* and anti-*Leishmania infantum* *in vitro* activity, cytotoxicity on VERO cells and selectivity towards the parasites. To study the antiparasitic properties of the new Mn(I) tricarbonyls, the EC$_{50}$ values of the compounds and free ligands were determined using viability assays after parasite incubation with increasing concentrations of the tested compounds. All EC$_{50}$ values for the Mn(I) compounds on *T. cruzi* epimastigotes and trypomastigotes, and *L. infantum* promastigotes resulted in the low micromolar range. Most compounds showed 2–6 fold higher activity on trypomastigotes of *T. cruzi* compared with the reference antitrypanosomal drug Nifurtimox (Nifurtimox EC$_{50}$ epimastigotes: 2.43 ± 0.51 μM; EC$_{50}$ trypomastigotes: 3.35 ± 0.87 μM, both determined through the same technique on the same parasite strain used in this work).[30]

As depicted in Table 1, the coordination of CTZ to the manganese(I) tricarbonyl centre resulted in an increase in antiparasitic activity as evidenced by a decrease in the EC$_{50}$ value by one order of magnitude when compared with the free CTZ. This behaviour was observed in both *T. cruzi* parasitic forms, as well as in *L. infantum* promastigotes. Additionally, similar EC$_{50}$ values were observed in both trypanosomatid parasites,

Table 1 *In vitro* activity on *T. cruzi* (Dm28c clone) epimastigotes and trypomastigotes, *L. infantum* promastigotes and VERO cells

Compound	EC_{50} *T. cruzi* epimastigotes ± SD (μM)	EC_{50} *T. cruzi* trypomastigotes ± SD (μM)	EC_{50} *L. infantum* promastigotes ± SD (μM)	EC_{50} VERO cells ± SD (μM)
CTZ	22.2 ± 0.5[a]	14.8 ± 2.9	6.24 ± 0.16	37.1 ± 7.6[a]
Phen	10.2 ± 0.3[a]	0.35 ± 0.07[b]	>10	50.2 ± 18.7[a]
Aminophen	9.37 ± 1.02[a]	1.29 ± 0.47	>10	29.9 ± 4.3[a]
tmp	3.43 ± 0.85[a]	0.24 ± 0,02[b]	ND[c]	51.9 ± 10.2[a]
bipy	12.5 ± 0.8[a]	>10[b]	>10	81.3 ± 14.0[a]
dmb	10.6 ± 2.4[a]	>10	>10	95.2 ± 17.0[a]
$[Mn(CO)_3(CTZ)(phen)](PF_6)$	1.04 ± 0.20	1.84 ± 0.13	2.32 ± 0.25	3.91 ± 0.22
$[Mn(CO)_3(CTZ)(aminophen)](PF_6)$	3.11 ± 1.53	4.46 ± 0.55	2.91 ± 0.31	7.02 ± 0.51
$[Mn(CO)_3(CTZ)(tmp)](PF_6)$	0.81 ± 0.11	0.59 ± 0.04	0.80 ± 0.11	2.11 ± 0.14
$[Mn(CO)_3(CTZ)(bipy)](PF_6)$	3.00 ± 1.18	1.95 ± 0.09	2.46 ± 0.11	4.53 ± 0.47
$[Mn(CO)_3(CTZ)(dmb)](PF_6)$	2.61 ± 1.52	0.88 ± 0.04	1.85 ± 0.19	2.28 ± 0.25
$[Re(CO)_3(CTZ)(phen)](PF_6)$	9.42 ± 1.53[a]	0.46 ± 0.20	—	3.20 ± 0.24[a]
$[Re(CO)_3(CTZ)(aminophen)](PF_6)$	8.43 ± 2.20[a]	0.57 ± 0.05	—	12.8 ± 2.2[a]
$[Re(CO)_3(CTZ)(tmp)](PF_6)$	3.48 ± 0.98[a]	0.25 ± 0.05	—	5.10 ± 1.60[a]
$[Re(CO)_3(CTZ)(bipy)](PF_6)$	7.53 ± 2.68[a]	1.36 ± 0.12	—	6.50 ± 1.10[a]
$[Re(CO)_3(CTZ)(dmb)](PF_6)$	8.48 ± 1.46[a]	0.51 ± 0.18	—	14.0 ± 4.3[a]

[a] Data from ref. 29 using the same technique. [b] Data from ref. 28 using the same technique. [c] ND – not determined.

Table 2 Selectivity index values towards the parasites in *T. cruzi* epimastigotes and trypomastigotes, and *L. infantum* promastigotes

Compound	SI[a] *T. cruzi* epimastigotes	SI[a] *T. cruzi* trypomastigotes	SI[a] *L. infantum* promastigotes
$[Mn(CO)_3(CTZ)(phen)](PF_6)$	3.8	2.1	1.7
$[Mn(CO)_3(CTZ)(aminophen)](PF_6)$	2.3	1.6	2.4
$[Mn(CO)_3(CTZ)(tmp)](PF_6)$	2.6	3.6	2.6
$[Mn(CO)_3(CTZ)(bipy)](PF_6)$	1.5	2.3	1.8
$[Mn(CO)_3(CTZ)(dmb)](PF_6)$	0.9	2.6	1.2
$[Re(CO)_3(CTZ)(phen)](PF_6)$	0.34[b]	6.9	—
$[Re(CO)_3(CTZ)(aminophen)](PF_6)$	1.5[b]	22.4	—
$[Re(CO)_3(CTZ)(tmp)](PF_6)$	1.5[b]	20.4	—
$[Re(CO)_3(CTZ)(bipy)](PF_6)$	0.89[b]	8.8	—
$[Re(CO)_3(CTZ)(dmb)](PF_6)$	1.6[b]	27.4[b]	—

[a] SI = EC_{50} VERO/EC_{50} parasite. [b] Data from ref. 29 using the same technique.

in agreement with our design hypothesis. $[Mn(CO)_3(CTZ)(tmp)](PF_6)$ was the most active compound on both parasites, *T. cruzi* and *L. infantum*.

For *T. cruzi* epimastigotes and in most cases for *T. cruzi* trypomastigotes, Mn(I) compounds showed an increase in the biological activity when compared with the free NN ligands. In the case of *L. infantum* promastigotes, only free CTZ showed EC_{50} values lower than 10 μM, whereas all Mn(I) compounds were active (EC_{50}: 0.80–2.46 μM), demonstrating improved biological activity. Regarding the selectivity, no significant improvements were found between the free ligands and the Mn(I) compounds (Table 2). The Mn compounds exhibited similar selectivity indexes (SI) values for *T. cruzi* and *L. infantum* (Table 2).

When compared with their Re(I) analogues, the Mn(I) compounds showed similar activity against both *T. cruzi* epimastigotes and trypomastigotes (Table 2). Moreover, for both metal centres the most active and selective organometallic compound on this parasite was the one with NN = tmp. *fac*-$[Mn(CO)_3(CTZ)(tmp)](PF_6)$ was also the most active compound of the series on *L. infantum*. Against initial expectations, the Mn(I) compounds showed higher unspecific cytotoxicity (VERO cells) than the Re(I) analogues, leading to lower selectivity index values towards the relevant trypomastigote form of this parasite (Table 2).[29]

Stability in solution

In the early stages of the process of design and development of potential metal-based drugs, the analysis and optimization of stability plays a very important role.[86]

To obtain initial information of the stability of the synthesized compounds, *in vitro* analyses by HPLC-DAD were performed by incubating the final compounds in different media of biological relevance.[67]

The stability of the five *fac*-$[Mn(CO)_3(CTZ)(NN)](PF_6)$ compounds was studied in three different media: DMSO, DMSO : BHI supplemented with 10% FBS (50 : 50), and DMSO : FBS (50 : 50), the latter as a model for mammalian serum.

Chromatograms obtained at the initial time (t_1) and later times were compared by evaluating the shapes and the area of the chromatographic peaks. As well, chromatograms were com-

pared against the ones of the free ligands, independently injected under the same chromatographic conditions.

Retention times of the compounds did not vary significantly in the different assayed media. The values were between 22 and 28 min for the studied Mn(I) compounds, higher than those for the free ligands, which were in the range of 14–22 min.[29]

In DMSO media, all five compounds were stable during a 24 h period, showing no significant changes in retention times or alterations in the peak shape and area. For NN = phen and tmp, the compounds remained stable during a 5-day period, but for NN = bipy, dmb and aminophen, signs of decomposition were detected.

In mixtures including culture media and mammalian serum, all compounds showed signs of decomposition since t_1, but later the general profile of the chromatogram remained the same over 24 h. This may be an indicator of a quick equilibrium reached by the organometallic compounds in the complex media studied by substitution of CTZ for other components of the media. This was verified by comparing the chromatograms of each compound and CTZ alone in the relevant media. Substitution of NNs was not detected, at least at this early stage. Obtained chromatograms are shown for *fac*-[Mn(CO)$_3$(CTZ)(tmp)](PF$_6$) (Fig. S24†). The Re(I) analogues showed better stability than the Mn(I) ones, all five NN derivatives being stable for 5 days in DMSO, and for 24 h in DMSO : BHI 50 : 50 and DMSO : FBS 50 : 50.[29]

Lipophilicity

Lipophilicity is a critical property of bioactive molecules, as it significantly influences the behavior in biological systems. It plays a key role in determining a compound's ability to penetrate biological membranes. Furthermore, lipophilicity is essential in pharmacokinetics, as it profoundly impacts the absorption, distribution, excretion, and toxicity of potential drug candidates.[69,87,88]

Therefore, it is an important property in the design of new drugs, being relevant to determine if there is a correlation between the lipophilicity of a series of compounds and their biological activity.

RP-HPLC has been used as a tool for the assessment of lipophilicity, since the hydrophobic forces dominate the retention process. This technique has been proved useful for the study of complex systems, in which the separation of multiple compounds is difficult by batch thin-layer chromatography methods, and more practical than octanol–water partition.[69]

The chromatographic conditions used for the analysis of the Re(I) analogues, previously reported by our research group, were proved useful for the Mn(I) compounds. The retention times (t_R) of the complexes were between 19 and 48 min (Table 3 and Fig. 3). Hold-up time (t_0) was measured through t_R of tartrazine, 2.709 min, compound that does not interact with the reverse-phase column. The parameters t_0 and t_R were used to calculate R_F and R_M parameters, according to reports from Bate-Smith and Westall, with t_c being the total time of the run, in this case of 55 min, following the equations described below:

$$R_F = (t_R - t_0)/t_c \quad (4)$$

$$R_M = \log(1/R_F - 1) \quad (5)$$

According to the obtained results, for the Mn(I) compounds the lipophilicity order of the series is *fac*-[Mn(CO)$_3$(CTZ)(phen)](PF$_6$) < *fac*-[Mn(CO)$_3$(CTZ)(bipy)](PF$_6$) < *fac*-[Mn(CO)$_3$(CTZ)(aminophen)](PF$_6$) < *fac*-[Mn(CO)$_3$(CTZ)(dmb)](PF$_6$) < *fac*-[Mn(CO)$_3$(CTZ)(tmp)](PF$_6$) (Fig. 3). As expected, for the same NN skeleton, the addition of methyl groups increases the lipophilicity (NN = phen < tmp, and bipy < dmb), and this effect is higher for phen and tmp, where the amount of methyl groups increases significantly the lipophilicity of the compound. With the exception of *fac*-[Mn(CO)$_3$(CTZ)(aminophen)](PF$_6$), an approximate relationship between lipophilicity and anti-*T. cruzi* and anti *L. infantum* activity was found: the higher the lipophilicity, the more active the compound. The most active compound on both parasites, *fac*-[Mn(CO)$_3$(CTZ)(tmp)](PF$_6$), is the most lipophilic one of the series.

Table 3 Chromatographic parameters t_R, R_F and R_M obtained for each compound

Compound	t_R (min)	R_F	R_M
Tartrazine	2.709	—	—
fac-[Mn(CO)$_3$(CTZ)(phen)](PF$_6$)	19.31	0.301	0.364
fac-[Mn(CO)$_3$(CTZ)(bipy)](PF$_6$)	19.34	0.302	0.363
fac-[Mn(CO)$_3$(CTZ)(aminophen)](PF$_6$)	24.91	0.404	0.169
fac-[Mn(CO)$_3$(CTZ)(dmb)](PF$_6$)	27.09	0.443	0.099
fac-[Mn(CO)$_3$(CTZ)(tmp)](PF$_6$)	47.73	0.819	−0.654
fac-[Re(CO)$_3$(CTZ)(phen)](PF$_6$)[a]	14.82	0.206	0.585
fac-[Re(CO)$_3$(CTZ)(bipy)](PF$_6$)[a]	18.92	0.281	0.442
fac-[Re(CO)$_3$(CTZ)(aminophen)](PF$_6$)[a]	25.41	0.399	0.178
fac-[Re(CO)$_3$(CTZ)(dmb)](PF$_6$)[a]	18.09	0.266	0.442
fac-[Re(CO)$_3$(CTZ)(tmp)](PF$_6$)[a]	29.28	0.451	0.086

[a] t_R values reported in ref. 29. R_F and R_M values were recalculated using the t_c of 55 minutes, so Mn(I) and Re(I) analogues could be compared.

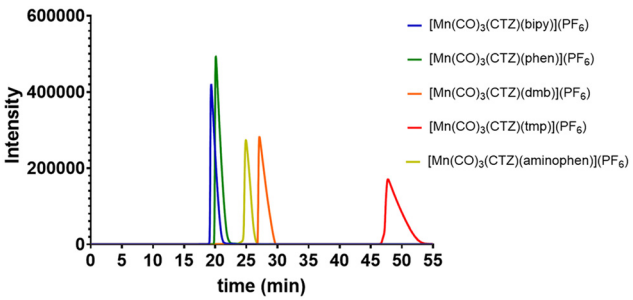

Fig. 3 Chromatogram obtained for the mixture of the five Mn-CTZ-NN compounds: *fac*-[Mn(CO)$_3$(CTZ)(phen)](PF$_6$), *fac*-[Mn(CO)$_3$(CTZ)(dmb)](PF$_6$), *fac*-[Mn(CO)$_3$(CTZ)(bipy)](PF$_6$), *fac*-[Mn(CO)$_3$(CTZ)(aminophen)](PF$_6$), *fac*-[Mn(CO)$_3$(CTZ)(tmp)](PF$_6$).

For comparing the Mn(I) and Re(I) analogues, the R_F values previously reported for the Re(I) compounds had to be recalculated with the t_c of the assay with Mn, so all compounds could be included into the analysis.

For all NN ligands, the Mn(I) compound was found to be more lipophilic than the Re(I) one, which could be explained because Mn(I), being smaller than Re(I), creates smaller coordination compounds with the same ligands. However, for the case of NN = tmp, the difference in lipophilicity was bigger than expected with this reasoning. Because of that, computational studies were carried out to get more insight into the difference between both families of compounds.

Computational insights into lipophilicity of analogues Re and Mn final compounds

log *P* values for the tricarbonyl complexes were computationally estimated using density functional theory (DFT). To identify the optimal level of theory, an initial screening was conducted on the *fac*-[Re(CO)$_3$(CTZ)(phen)]$^+$ species, which has a known crystalline structure and an experimental log *P* value. This screening employed six different functionals and four basis sets within the SMD implicit solvation model. The results, depicted in Fig. S25a and in Tables S2 and S3,† revealed that absolute errors in calculated log *P* (log P_{calc}) relative to experimental values (log P_{exp}) were highly dependent on the functional and basis set. The best-performing combinations included LANL2DZ with B3LYP, M06L, ωB97XD, and PBE0 functionals.

Using these four combinations, the log *P* values for the other Re(I) complexes were computed, excluding the Re-aminophen compound, for which no experimental log *P* value is available (see Fig. S25b and Table S3†). The theoretical log *P* trends were consistent with experimental values, with M06L/LANL2DZ and ωB97XD/LANL2DZ providing the lowest root-mean-square errors (RMSEs) across all systems—0.71 and 0.61, respectively (Fig. S25c and d†). These two methods were then applied to the Mn(I) complexes (see Table S4†).

Special consideration was given to the aminophen complexes, as their theoretical log *P* values deviated from experimental ones. This discrepancy likely arose from strong hydrogen bonding between the amino substituent and the solvent. To address this, two explicit water molecules were added to the SMD solvation model as hydrogen-bond acceptors for the amino group. This enhanced model significantly improved the agreement between calculated and experimental results (see Table S5†).

Based on the optimized computational approach, Table S6† presents log P_{calc} values for all complexes using M06L/LANL2DZ and ωB97XD/LANL2DZ. As expected, a near-linear negative correlation was observed between log P_{calc} and R_M values for Re(I) and Mn(I) complexes (R^2 = 0.72–0.97; Fig. S26†). A single outlier, *fac*-[Re(CO)$_3$(CTZ)(bipy)]$^+$, exhibited lipophilicity that deviated from the general trend. Overall, both experimental and computational data confirmed that Mn(I) tricarbonyl complexes are more lipophilic than their Re(I) analogues.

To gain insights into the structural and electronic basis behind this trend, Fig. 4 illustrates a comparative computational analysis of charge distributions. Mn(I) complexes consistently displayed lower dipole moments than their Re(I) counterparts (*e.g.*, Fig. 4b for *fac*-[Re(CO)$_3$(CTZ)(phen)]$^+$ *vs.* *fac*-[Mn(CO)$_3$(CTZ)(phen)]$^+$). This reduction in dipole moment is attributed to a redistribution of the electrostatic potential (ESP) near the Mn(I) center, leading to decreased overall

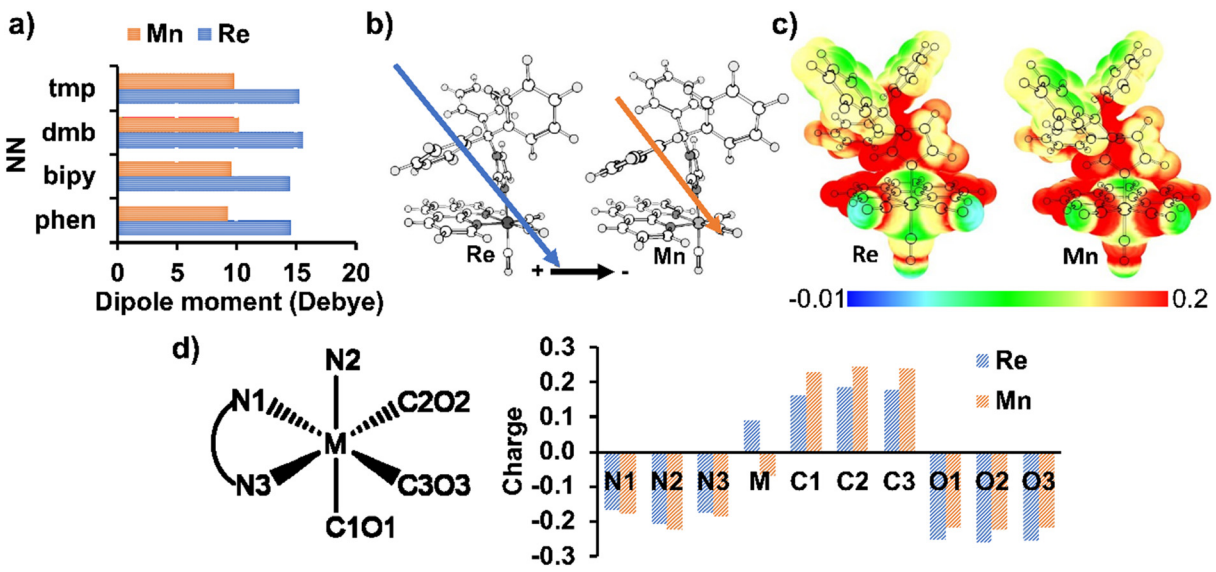

Fig. 4 (a) Dipole moment magnitudes of the Mn(I) and Re(I) tricarbonyl complexes (NN = phen, bipy, dmb, tmp). (b) Dipole moment vectors of the *fac*-[Re(CO)$_3$(CTZ)(phen)]$^+$ and *fac*-[Mn(CO)$_3$(CTZ)(phen)]$^+$ species. (c) Electrostatic potential surfaces (ESP) of the *fac*-[Re(CO)$_3$(CTZ)(phen)]$^+$ and *fac*-[Mn(CO)$_3$(CTZ)(phen)]$^+$ species (isosurface value = 0.004*e*). (d) DDEC6 atomic charges for the coordination centers, N donor atoms, and carbonyl groups. Level of theory: ωB97XD-SMD/LANL2DZ.

charge polarization (Fig. 4c). The DDEC6 atomic charges (Fig. 4d) reveal a shift in electron density from the CO ligands to the Mn(NN) core during the transition from Re(I) to Mn(I) species, accounting for both the diminished dipole moment and the enhanced lipophilicity of Mn(I) complexes.

Even though the difference in the dipole moment between both families of complexes is associated with the global change in lipophilicity, the individual dipole values show no obvious correlation with experimental log *P* values. To unveil the determinants of lipophilicity trends within each family, the molecular polarity index (MPI) was explored, which measures the distribution of positive and negative potential across a molecular surface.[89]

Interestingly, MPI does have a positive correlation with R_M, being a good descriptor of lipophilicity (R^2 = 0.72; Fig. 5). This indicates that the balance of polar and nonpolar surface areas plays a significant role in determining lipophilicity. Indeed, according to Table S7,† the Re(I) complexes containing phen, bipy, or dmb ligands have smaller nonpolar surface areas and lower R_M values, making them less lipophilic. In contrast, compounds with NN = tmp and aminophen exhibit larger nonpolar surface areas, contributing to higher lipophilicity. Notably, the compound with NN = aminophen exhibits the highest molecular dipole moment, rendering it significantly more polar and hydrophilic than the tmp analogue, despite the latter possessing a smaller nonpolar surface area.

Insight into the mechanism of action

DNA interaction studies. DNA has been proposed as a potential molecular target of the Mn(I) tricarbonyl compounds developed, given the presence of the polypyridyl NN ligand.

Fluorescence quenching studies were performed to study this interaction. Ethidium bromide (EB) was employed to get indirect information about the interaction between the Mn(I) compounds and DNA, by competition for DNA with EB on a preformed {DNA-EB} adduct. Under the selected experimental conditions, EB shows an emission maximum at 607 nm for an excitation wavelength of 510 nm. Intercalation of the dye into double-stranded DNA causes an increase of the fluorescence quantum yield and a shift of the emission maximum.[90]

Under the experimental conditions, the emission maximum of the {DNA-EB} adduct is located at 597 nm for the 510 nm excitation wavelength. In these excitation–emission conditions, the *fac*-[Mn(CO)$_3$(CTZ)(NN)](PF$_6$) compounds lack intrinsic fluorescence in 10 mM Tris-HCl pH = 7.4 buffer solution–5% DMSO, and no fluorescence emission was found when incubating the compounds with DNA alone. The fluorescence intensity was corrected by the compounds' absorption at 510 and 597 nm. The interaction between the compounds and {DNA-EB} led in all cases except for NN = aminophen to the displacement of EB from the adduct, which was evidenced by a decrease in the intensity of fluorescence at {DNA-EB} maximum of emission in a concentration-dependent manner.

With the quenching of fluorescence, a Stern–Volmer analysis was conducted to indirectly quantify the strength of the interaction (eqn (1)) (Table 4 and Fig. S27†).

*K*sv values were similar or lower than those previously reported for Pd and Pt complexes showing antitrypanosomal activity, and for other complexes with typical planar DNA intercalating ligands.[68,91–93]

The obtained values indicate a moderate interaction of the compounds with DNA and the strength of the interaction does not correlate with the observed antiparasitic activity. Although DNA could be postulated as a potential molecular target of the compounds, it should not be considered the primary one.

Inhibition of the biosynthesis of membrane sterols

Ergosterol is essential for maintaining the structure and normal function of microbial membranes. Various drugs targeting sterol biosynthesis have been used to treat fungal infections, with some also evaluated for their antiparasitic activity against *Trypanosoma brucei*, *Trypanosoma cruzi*, and *Leishmania* species. Notably, ergosterol biosynthesis in *T. cruzi* has been identified as a promising chemotherapeutic target, with multiple enzymes in the pathway—such as squalene-2,3-epoxidase, lanosterol synthase, and lanosterol 14-α-demethylase—being susceptible to inhibition. Azoles like CTZ are potent inhibitors of C14 α-demethylase (CYP51), a key enzyme in this pathway.[46,47,94]

To investigate CYP51 as a potential target in the ergosterol biosynthetic pathway, the concentrations of ergosterol and its precursors in the pathway lanosterol, and squalene, were quantified in control parasites and those treated with

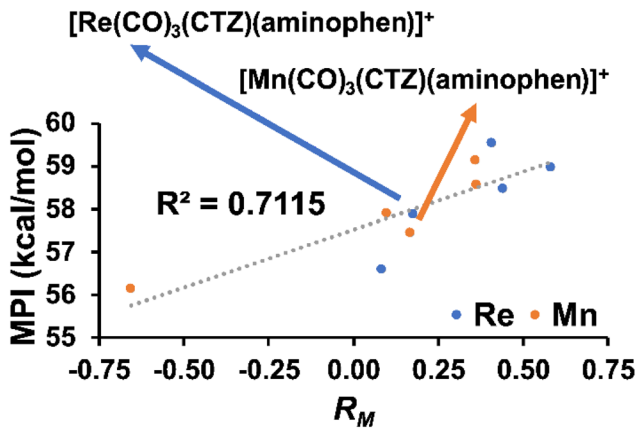

Fig. 5 MPI (calculated at ωB97XD-SMD/LANL2DZ level of theory) *vs.* R_M for the tricarbonyl complexes.

Table 4 Stern–Volmer constants of the *fac*-[Mn(CO)$_3$(CTZ)(NN)](PF$_6$) compounds for the competitive binding to {DNA-EB} adduct in 5% DMSO-Tris HCl medium

Compound	K_{SV} (M^{-1})	log (K_{SV})
fac-[Mn(CO)$_3$(CTZ)(bipy)](PF$_6$)	6293	3.80
fac-[Mn(CO)$_3$(CTZ)(phen)](PF$_6$)	5776	3.76
fac-[Mn(CO)$_3$(CTZ)(dmb)](PF$_6$)	3869	3.59
fac-[Mn(CO)$_3$(CTZ)(tmp)](PF$_6$)	1184	3.07

Table 5 Ergosterol, lanosterol and squalene quantification in *T. cruzi* epimastigotes and *L. infantum* promastigotes after 4 h of incubation with *fac*-[Mn(CO)$_3$(CTZ)(tmp)](PF$_6$)

	Control	1× EC_{50}			5× EC_{50}		
Sterol	*C* (μM)	*C* (μM)	*A* (%)	*D* (%)	*C* (μM)	*A* (%)	*D* (%)
***T. cruzi* epimastigotes**							
Ergosterol	11.45 ± 0.75	9.09 ± 0.40	—	21.1	8.56 ± 0.52	—	25.2
Lanosterol	6.54 ± 0.30	7.39 ± 0.29	13.0	—	8.47 ± 0.60	29.5	—
Squalene	12.27 ± 0.71	13.04 ± 0.65	6.3	—	13.45 ± 0.81	9.6	—
***L. infantum* promastigotes**							
Ergosterol	15.35 ± 0.92	11.22 ± 0.84	—	26.9	11.01 ± 0.84	—	28.3
Lanosterol	5.03 ± 0.20	6.01 ± 0.30	19.5	—	6.64 ± 0.33	32.0	—
Squalene	9.77 ± 0.58	10.65 ± 0.73	9.0	—	10.93 ± 0.91	11.9	—

A (%): accumulation percentage, *D* (%): depletion percentage.

fac-[Mn(CO)$_3$(CTZ)(tmp)](PF$_6$), the most active compound of the series.

As shown in Table 5, treatment of both parasites, *T. cruzi* and *L. infantum*, with the selected compound led to the accumulation of lanosterol and squalene, accompanied by ergosterol depletion at both tested concentrations compared with untreated parasites. The accumulation of lanosterol and depletion of ergosterol were more pronounced at 5× EC_{50} than at 1× EC_{50}, suggesting a dose-dependent effect.

The accumulation of lanosterol and depletion of ergosterol observed by treatment of both parasites with *fac*-[Mn(CO)$_3$(CTZ)(tmp)](PF$_6$) suggests that the compound may inhibit activity of the enzyme lanosterol 14-α-demethylase, as has been reported for the free ligand CTZ.[29,95]

When compared with free CTZ, previously evaluated using the same method, the Mn compound exhibited slightly higher percentages of lanosterol accumulation and ergosterol depletion. This suggests that *fac*-[Mn(CO)$_3$(CTZ)(tmp)](PF$_6$) may have slightly greater inhibitory activity than the free ligand. However, the observed effect could also be due to the combination of free CTZ and the complex, as the metal compound may act as a CTZ carrier.

Previously reported results for the Re(I) analogue, *fac*-[Re(CO)$_3$(CTZ)(tmp)](PF$_6$), using the same method on *T. cruzi*, indicate a slightly stronger inhibitory effect compared with the Mn compound.[29]

CO release studies

The antimicrobial mechanisms of action of *fac*-[M^{I}(CO)$_3$]$^+$ species are diverse and remain only partially understood. In this sense, CO release by carbonyl compounds can be triggered by physical, chemical or enzymatic processes.[40,58,96,97]

Although the therapeutic potential of CO is gaining recognition in the development of antibacterial agents, CORMs remain largely unexplored as antitrypanosomal agents. As a first approach, the photoinduced CO release behavior of the analogous Re(I) and Mn(I) tricarbonyl compounds developed in our studies was compared.

Photoinduced CO release occurs when there is an overlapping of the wavelength of the light used and the MLCT band of the carbonylic compound. Therefore, 395 ± 10 nm was chosen to promote the release of the CO ligands.

CO release studies performed using FTIR spectroscopy revealed that all compounds release CO upon irradiation at a wavelength of 395 ± 10 nm (Fig. 6 and Fig. S28–31†). This release is evident from a decrease in the intensity of the tricarbonyl center stretching bands (2050–1900 cm^{-1}), together with the appearance of a band near 2143 cm^{-1} corresponding to free carbon monoxide. Additionally, changes in the relative intensities of the bands between 1975–1925 cm^{-1}, along with the appearance of new bands in the 1875–1850 cm^{-1} region, indicate the formation of stable biscarbonyl species. However, in some cases, analysis is complicated by the overlap of the asymmetric tricarbonyl bands with the symmetric biscarbonyl band.[57]

CO release studies conducted using UV-Vis spectroscopy demonstrated a decrease in the absorbance of the MLCT band (358–392 nm) upon irradiation at a wavelength of 395 ± 10 nm, confirming CO release. The presence of isosbestic points suggests the formation of other species in equilibrium with the initial tricarbonyl complexes. In some cases (NN = bipy, dmb, aminophen), a decrease in the absorbance of the intrali-

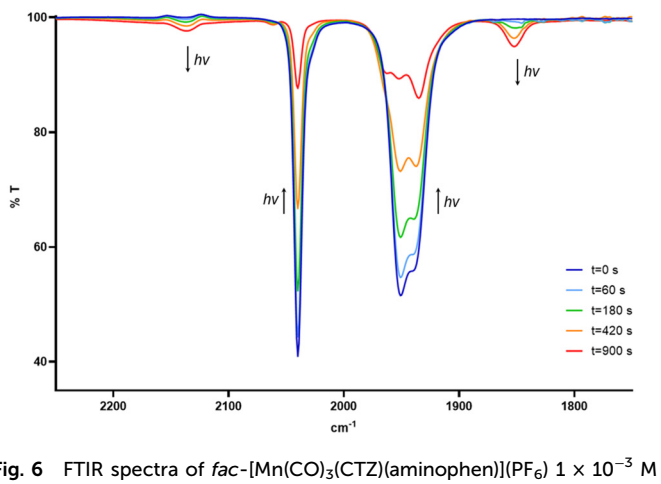

Fig. 6 FTIR spectra of *fac*-[Mn(CO)$_3$(CTZ)(aminophen)](PF$_6$) 1 × 10^{-3} M in CH_2Cl_2 solution after 0–900 s irradiation at 395 ± 10 nm.

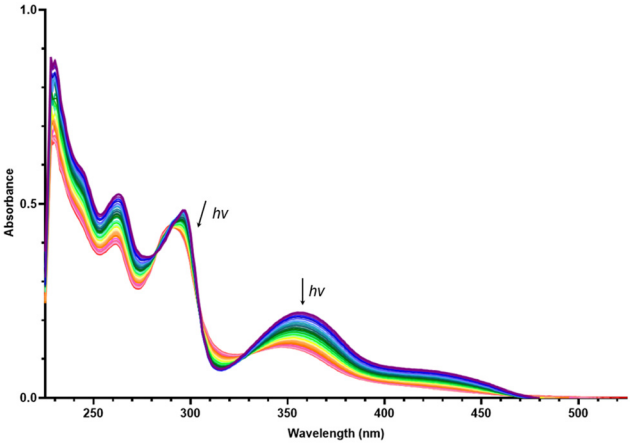

Fig. 7 UV-Vis spectra of *fac*-[Mn(CO)$_3$(CTZ)(aminophen)](PF$_6$) in CH_2Cl_2 solution after 0–3000 s irradiation at 395 ± 10 nm.

gand π → π* bands (228–233 nm and 288–297 nm) was observed, implying that the ligands remain bound to the manganese center in the photodecomposition product (Fig. 7 and Fig. S32, S33†). Conversely, in other cases (NN = phen, tmp), an increase in the absorbance of the intraligand π → π* bands (232 nm and 267–275 nm) was detected, suggesting that the ligands are released alongside CO upon irradiation (Fig. 8 and Fig. S34†).

The data showed a linear relationship between ln[C] (*C* = concentration of the compound) and irradiation time (Fig. S35†), indicating a first-order kinetic process. The *pseudo*-first-order CO release constants (k_{CO}) are presented in Table 6. These values are of a similar magnitude to those reported for other Mn(I) tricarbonyl complexes in the literature, highlighting consistency with previously observed CO release kinetics.[56,57,79,98]

Although no direct correlation was observed between the k_{CO} and the biological activity of the compounds, it is noteworthy that the most active compound,

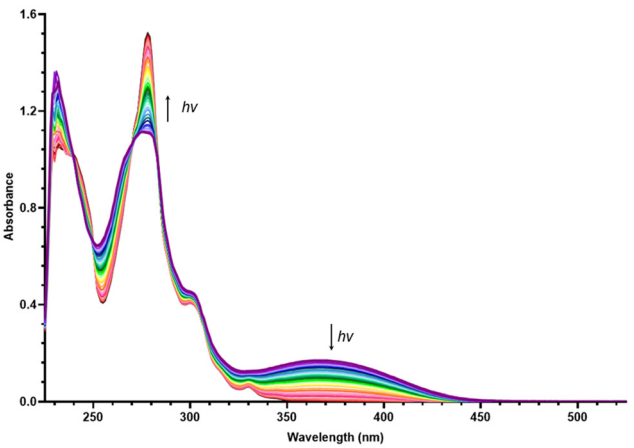

Fig. 8 UV-Vis spectra of *fac*-[Mn(CO)$_3$(CTZ)(tmp)](PF$_6$) in CH_2Cl_2 solution after 0–3060 s irradiation at 395 ± 10 nm.

Table 6 k_{CO} values for the *fac*-[Mn(CO)$_3$(CTZ)(NN)](PF$_6$) compounds

Compound	$k_{CO} \times 10^3 \pm$ SD (s^{-1})
fac-[Mn(CO)$_3$(CTZ)(bipy)](PF$_6$)	1.2 ± 0.1
fac-[Mn(CO)$_3$(CTZ)(phen)](PF$_6$)	0.82 ± 0.02
fac-[Mn(CO)$_3$(CTZ)(dmb)](PF$_6$)	0.68 ± 0.05
fac-[Mn(CO)$_3$(CTZ)(tmp)](PF$_6$)	1.7 ± 0.3
fac-[Mn(CO)$_3$(CTZ)(aminophen)](PF$_6$)	1.4 ± 0.2

fac-[Mn(CO)$_3$(CTZ)(tmp)](PF$_6$), also exhibited the highest k_{CO}. This result may suggest CO release as an additional mechanism of action worthy of further investigation.

To enable a comparison between Re(I) and Mn(I) analogues, the same experiments were performed for the *fac*-[Re(CO)$_3$(CTZ)(NN)](PF$_6$) compounds. However, no CO release was observed, either by FTIR or UV-Vis spectroscopy, even after over 4 h of continuous irradiation. Attempts to induce CO release by irradiating at a wavelength of 254 ± 10 nm, where the compounds also showed electronic absorption, were also unsuccessful, indicating a fundamental difference in photoreactivity between the Re(I) and Mn(I) compounds, and the high stability of the rhenium compounds under light exposure.

To get insight into the CO-release in aqueous media in absence of light, the spectra of the Mn compounds were recorded in a 24 h span at a concentration of 0.5 mM in DMSO : buffer phosphate 40 mM pH 7.4 (50 : 50). No significant changes were observed in the UV-vis spectra between t = 0 h and t = 24 h, which can be interpreted as there being no relevant CO release occurring in the conditions of the assay (Fig. S36†).

Metallomics

The manganese compound with the most promising *in vitro* antiparasitic activity, *fac*-[Mn(CO)$_3$(CTZ)(tmp)](PF$_6$), was selected for metallomics analysis. To investigate its uptake by *T. cruzi* epimastigotes and trypomastigotes, two concentrations (1× EC_{50} and 10× EC_{50}, corresponding to 0.81 and 8.10 μM for epimastigotes, and 0.59 and 5.90 μM for trypomastigotes) and two incubation times (4 and 24 h) were tested. Untreated parasites served as the control.

The manganese taken up by the parasites or strongly bound (not removable by washing), and the manganese remaining in the culture medium, were quantified using ET-AAS. The average manganese content, based on three independent experiments, is presented in Table 7.

Table 7 Percentage of manganese taken up by *T. cruzi* epimastigotes and trypomastigotes

Compound concentration	% taken up by *T. cruzi* epimastigotes ± SD		% taken by up *T. cruzi* trypomastigotes ± SD	
	4 h	24 h	4 h	24 h
1× EC_{50}	2.9 ± 0.2	2.7 ± 0.3	3.9 ± 0.3	3.8 ± 0.3
10× EC_{50}	2.7 ± 0.1	2.8 ± 0.1	3.2 ± 0.2	3.0 ± 0.1

As shown in Table 7, the uptake of *fac*-[Mn(CO)$_3$(CTZ)(tmp)](PF$_6$) in epimastigotes did not vary across the different concentrations and incubation times tested. In trypomastigotes, the uptake at the 1× EC_{50} concentration was slightly higher than at the 10× EC_{50} concentration, although no significant differences were observed with varying incubation times. In comparison, trypomastigotes exhibited higher uptake percentage than epimastigotes, which aligns with the compound's greater activity in trypomastigotes (Table 1).

When compared with its Re(I) analogue, the Mn(I) compound showed an uptake more than twice that of the Re(I) compound.[29] This enhanced uptake by the parasite might be related to the higher lipophilicity of the Mn(I) compounds across all NN ligands tested, which may impact on the biological activity.

The manganese association with biomacromolecules such as RNA, DNA, and soluble proteins was investigated to assess the subcellular distribution of the compound *fac*-[Mn(CO)$_3$(CTZ)(tmp)](PF$_6$) within the parasites. For this, *T. cruzi* epimastigotes were incubated for 4 h with the compound at two concentrations (1× EC_{50} and 10× EC_{50}). After incubation, the different biomacromolecules, along with the insoluble fraction, were isolated, and the total manganese associated with each fraction was quantified using ET-AAS (Table 8).

A similar distribution pattern was observed across the different concentrations studied. Most of the compound taken up by the parasite was associated with soluble proteins, while a smaller fraction was found in the insoluble fraction. Only a small percentage of the compound was associated with nucleic acids, both RNA and DNA. Given the minimal distribution towards DNA (less than 1% in both conditions), despite a moderate interaction between the compounds and this molecular target (see above), DNA binding would not be considered the primary mechanism of action for the compounds.

Differences between 1× and 10× results were tested by a one-way analysis of variance (ANOVA) at a 5% significance level, showing statistically significant differences for soluble proteins and RNA.

When comparing this distribution pattern with that of the Re(I) analogue, both compounds show a similar primary distribution towards soluble proteins, with over 80% of the compound associated with soluble proteins for both metal compounds and concentrations studied. There are no statistically significant differences for the two analogue compounds regarding soluble proteins association, according to the ANOVA test at a 5% significance level, for 1× and 10×, respectively. Both compounds also exhibit more than 10% association with the insoluble fraction with a smaller percentage associated with nucleic acids. However, the behavior of the two compounds differs in their association with RNA. For Re(I), the association with RNA is comparable to that with DNA, whereas for Mn(I), the association with RNA is more than 15 times greater than that with DNA.[33]

Table 8 Percentage of manganese associated with the different isolated biomacromolecules after 4 h of treatment of epimastigotes of *T. cruzi* with 1× EC_{50} and 10× EC_{50} of *fac*-[Mn(CO)$_3$(CTZ)(tmp)](PF$_6$)

	% association ± SD	
Subcellular fraction	1× EC_{50}	10× EC_{50}
Soluble proteins	81.5 ± 6.4	85.2 ± 5.6
DNA	0.4 ± 0.1	0.2 ± 0.04
RNA	6.7 ± 1.3	3.5 ± 0.8
Insoluble fraction	11.3 ± 0.9	11.1 ± 0.9

Confocal Raman microscopy

A confocal Raman microscopy study was performed to analyze the effects of the *fac*-[Mn(CO)$_3$(CTZ)(tmp)](PF$_6$) taken up in the whole parasite.

According to the literature, Raman bands in the range of ~1650 cm^{-1} correspond to amide I C=O stretching mode (proteins and DNA, Fig. 9 red region), signals in the range of 1425/1475 cm^{-1} correspond to CH_2/CH_3 anti-symmetric methyl/methylene deformations (lipids, Fig. 9 blue region) and signals in the range of 1570/1580 cm^{-1} correspond to C=C stretching modes in purine bases (DNA/RNA, Fig. 9 red area). As previously reported, the signal at 1594 cm^{-1} observed in Fig. 9 (blue area) could be attributed to DNA in higher concentration and the red labels to membrane lipids. The prominent bands of the compound show an important overlap with signals coming from lipids, proteins and DNA, and due to its low concentration in the parasite, signals associated with ν(CO) stretching modes are not so pronounced in Raman spectroscopy for being detected in our experiments. Therefore, the analysis focused on the main changes occurring in treated parasites relative to untreated control parasites.

Comparing confocal Raman images obtained for parasites treated with the Mn(I) compound at concentrations equivalent to 1×, 5×, 10× the EC_{50} value for 4 h with untreated control parasites (Fig. 9), it can be observed that the signals associated with DNA suffer important changes in their colocalization along the parasite, being more diffuse for the sample treated with 10× EC_{50} in comparison with 5× EC_{50} and successively. These features were also reported in prior work by Soba *et al.*,[29] where it was observed that the signals associated with DNA underwent significant alterations in their colocalization along the parasite. This observation aligns with our hypothesis that the treatment with Mn(I) compounds might be affecting the dynamics of the parasite by ergosterol biosynthesis inhibition. Lipid metabolism plays a vital role not only in maintaining the integrity of the plasma membrane but also in supporting the functionality of internal organelles such as the mitochondria, endoplasmic reticulum, and the endosomal–lysosomal system. Disruptions in lipid biosynthesis can lead to significant alterations in the morphology and function of these organelles, with consequences for overall parasite viability.[99–101]

The increased fluidity found in our study might not be restricted to the plasma membrane but could also extend to internal organelles. The diffuse appearance of DNA signals may therefore indicate a loss of its proper localization, which

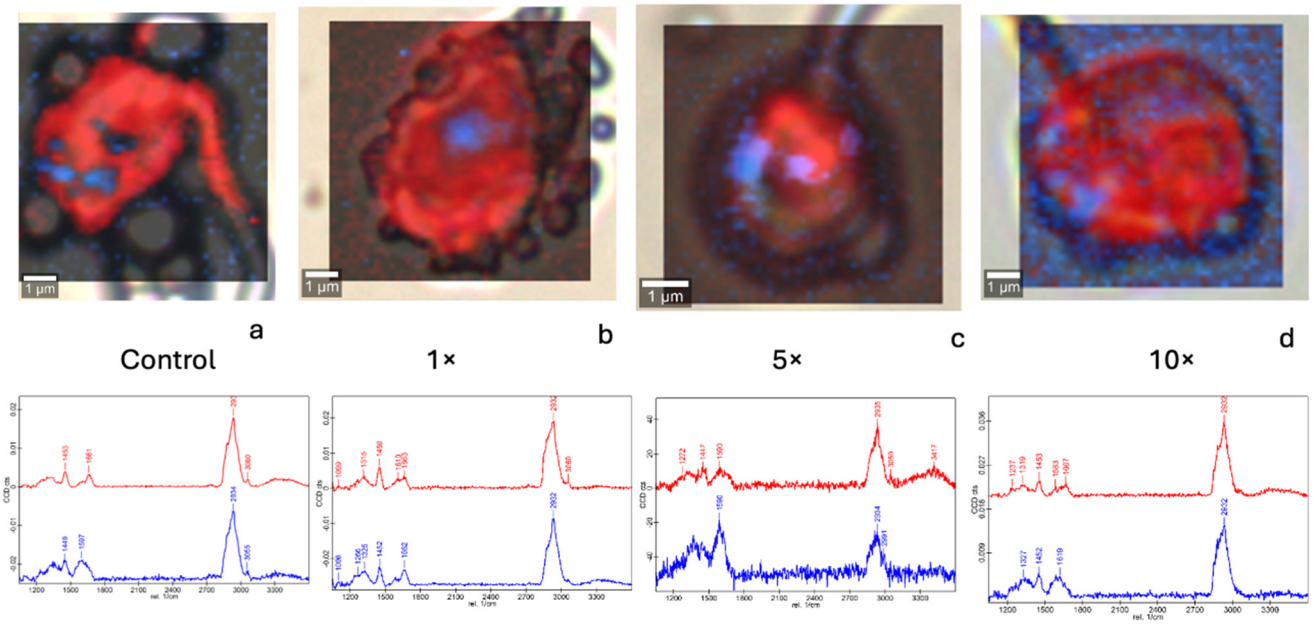

Fig. 9 (a) Overlay between optical and confocal Raman images as obtained from selected principal components analysis associated with lipids (red) and DNA (blue) and their corresponding Raman spectra for samples: (a) untreated control, (b) 1×, (c) 5× and (d) 10× the EC_{50} value of for *fac*-[$Mn(CO)_3$(CTZ)(tmp)](PF_6) for 4 h.

could be due to compromised organellar integrity and the alteration of lipid-dependent processes crucial for maintaining cellular compartmentalization. Therefore, while the observed changes in DNA signal colocalization are striking, they likely represent a more complex interplay of effects on various cellular processes that are crucial for *T. cruzi*'s survival and pathogenicity. Further studies are needed to confirm the precise mechanisms by which lipid metabolism alterations contribute to these changes and to understand how they relate to the overall therapeutic potential of the Mn(I) compound.

Proteomic studies

To further understand the mechanism of action of the most promising compound, *fac*-[$Mn(CO)_3$(CTZ)(tmp)](PF_6), in *T. cruzi*, the proteome of treated epimastigotes was analyzed using a concentration equivalent to 5 times the EC_{50} value (5× EC_{50}) previously calculated. To specifically identify proteins modulated in response to the compound, rather than general drug-response proteins, a treatment time of 4 h was used. For comparative purposes, the proteome of parasites treated with the analogue *fac*-[$Re(CO)_3$(CTZ)(tmp)](PF_6) was also analyzed in the same incubation conditions. As a control, untreated parasites were also analyzed.

Using the Venn diagram statistical module, 5 proteins were uniquely identified for the parasites treated with *fac*-[$Mn(CO)_3$(CTZ)(tmp)](PF_6), while 87 proteins were uniquely detected in the control samples, and 2110 proteins were found in both samples (p-value <0.05) (Fig. 10 and 11).

In comparison, for the parasites treated with *fac*-[$Re(CO)_3$(CTZ)(tmp)](PF_6) 47 proteins were uniquely identified, while 173 were uniquely detected in control samples and 1987 were found in both samples.

A pairwise comparison was performed for proteins detected in both conditions but exhibiting significant differences in relative abundance. Sixteen proteins with altered abundance were identified in *fac*-[$Mn(CO)_3$(CTZ)(tmp)](PF_6)-treated parasites, of which 4 proteins showed increased abundance, and 12 displayed decreased abundance compared with control samples. This number of proteins with altered abundance is significantly lower than the number obtained for the treatment with *fac*-[$Re(CO)_3$(CTZ)(tmp)](PF_6) using the same pairwise comparison analysis, where only 1 protein showed increased abundance in control samples and 455 proteins exhibited decreased abundance compared with control samples.

Gene ontology (GO) enrichment analyses were conducted on proteins with altered abundance to identify any functions or processes affected by the treatment. The categories "molecular function" and "biological process" were specifically examined. For downregulated proteins after *fac*-[$Mn(CO)_3$(CTZ)(tmp)](PF_6) treatment, the analysis revealed enrichment in proteins associated with protein modification processes, mitochondrial gene expression, cytoplasmic translation, RNA binding, and lipid binding (Table S9†).

No enriched terms were identified for upregulated proteins after treatment.

The GO term enrichment analysis for downregulated proteins in *T. cruzi* treated with *fac*-[$Re(CO)_3$(CTZ)(tmp)](PF_6) highlighted disruptions in broad biological processes, including the metabolism of amino acids, nucleobase-containing small molecules, carbohydrates, and modified amino acids, as well as processes related to energy generation and vitamin metab-

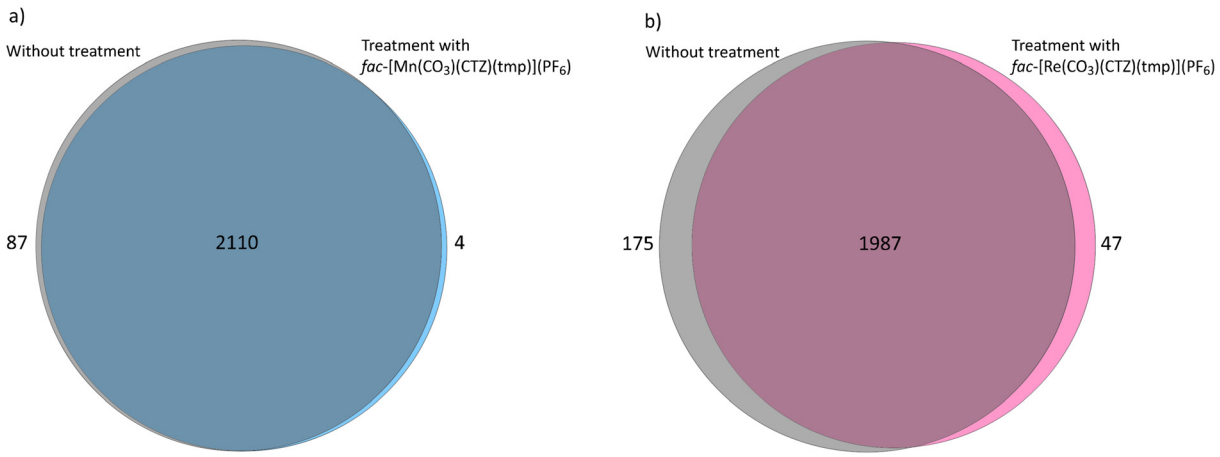

Fig. 10 Venn diagram displaying the overlap of proteins detected in *T. cruzi* epimastigotes treated with *fac*-[$Mn(CO)_3$(CTZ)(tmp)](PF_6) *versus* untreated control (a), and in *T. cruzi* epimastigotes treated with *fac*-[$Re(CO)_3$(CTZ)(tmp)](PF_6) *versus* untreated control. (b) The gray circles represent proteins uniquely identified in treated parasites, light blue circle show proteins exclusively detected in *fac*-[$Mn(CO)_3$(CTZ)(tmp)](PF_6)-treated samples (4 proteins) and pink circle represents proteins uniquely detected in *fac*-[$Re(CO)_3$(CTZ)(tmp)](PF_6)-treated samples. The overlapping region indicates proteins identified in both conditions. Statistical analysis was applied to determine significance (p-value <0.05). Details of protein identification are shown in ESI Table S8.†

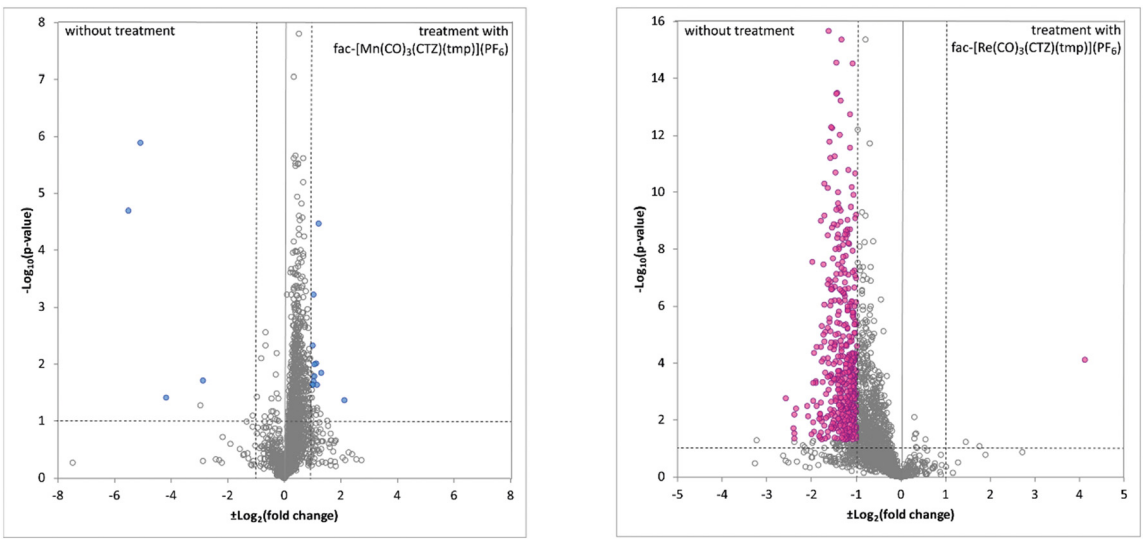

Fig. 11 Differentially abundant proteins between *T. cruzi* epimastigotes untreated and treated with *fac*-[$Mn(CO)_3$(CTZ)(tmp)](PF_6) (left panel) and *T. cruzi* epimastigotes untreated and treated with *fac*-[$Re(CO)_3$(CTZ)(tmp)](PF_6) (right panel). The volcano plots show the $-\log_{10}$ (p-value) on the y-axis and the $\log_2$ (fold-change) on the x-axis. Each dot represents a protein identified in both conditions. Blue and pink dots indicate proteins that satisfy all statistical criteria and are therefore considered differentially abundant between conditions. Dotted lines mark the cutoff thresholds for fold change ($\pm\log_2$ fold change = 1, corresponding to a fold change of ±2) and p-value ($\log_{10}$ p-value = 1, equivalent to p = 0.05). Details of protein identification are shown in Table S8.†

olism. Additionally, RNA-related functions such as tRNA and mRNA metabolism were affected, alongside protein-related activities including folding, modification, catabolism, and translation. Structural and transport processes, such as intracellular protein transport and cytoskeleton organization, were also impacted, underscoring the compound's broad influence on fundamental cellular functions. On the molecular function level, enrichment in binding activities such as ion binding, RNA binding, and cytoskeletal protein binding was observed. Additionally, key enzymatic functions were affected, including ligase, methyltransferase, phosphatase, GTPase, oxidoreductase, isomerase, and peptidase activities. Structural roles were also impacted, particularly with the enrichment of terms related to the structural constituents of ribosomes and structural molecule activities. These findings suggest broad disruptions in both enzymatic functions and structural integrity in *T. cruzi* cells treated with *fac*-[$Re(CO)_3$(CTZ)(tmp)](PF_6) (Table S10†).

The GO analysis of upregulated proteins in *T. cruzi* treated with *fac*-[Re(CO)$_3$(CTZ)(tmp)](PF$_6$) revealed enrichment in general biological processes such as cytoskeleton organization, protein-containing complex assembly, anatomical structure development, carbohydrate metabolic process, and mRNA metabolic process. These processes highlight extensive cellular functions influenced by the compound, pointing to its impact on structural organization, metabolic activity, and protein synthesis machinery. On the molecular function side, an enrichment in methyltransferase activity and cytoskeletal protein binding was observed (Table S11†). These functions suggest an influence on protein modification and structural interactions within the cell, potentially affecting regulatory processes and cellular architecture.

In conclusion, the biological processes and molecular functions altered in *T. cruzi* parasites treated with both Re- and Mn-based compounds were broad and nonspecific, making it challenging to identify a precise metabolic pathway or process directly impacted by the treatments. These findings suggest that the compounds induce a general cellular response, potentially affecting multiple pathways rather than selectively targeting a distinct biological process. It is also noteworthy that a significant portion of the identified proteins were "uncharacterized proteins", complicating the analysis. Specifically, 24% (pairwise comparison analysis) and 14% (Venn diagrams) of the total proteins identified in *fac*-[Mn(CO)$_3$(CTZ)(tmp)](PF$_6$)-treated samples and 8% (pairwise comparison) and 17% (Venn diagrams) of the *fac*-[Re(CO)$_3$(CTZ)(tmp)](PF$_6$)-treated samples fell into this category.

Since it was demonstrated in this paper that treatment with *fac*-[Mn(CO)$_3$(CTZ)(tmp)](PF$_6$) leads to the accumulation of intermediates in the ergosterol pathway and a decrease in the amount of the final product, ergosterol, we hypothesized that perhaps one or more of the enzymes in this pathway may have altered abundance due to the treatment. However, proteomic analysis showed no differences in the abundance of these enzymes in treated parasites compared with control untreated parasites in the conditions tested (Table S12†). Thus, the accumulation of intermediates and the decrease in ergosterol levels might result from changes in post-translational modifications of some of these enzymes. In this context, among the proteins with altered abundance we could identify methyltransferases, phosphatases, and kinases, which could modify the activity of these ergosterol pathway proteins without changing their abundance.

Conclusions

Searching for new prospective drugs against *Trypanosoma cruzi*, the causative agent of Chagas disease, and *Leishmania infantum*, causative agent of visceral leishmaniasis, five heteroleptic multifunctional Mn(I) tricarbonyls *fac*-[Mn(CO)$_3$(CTZ)(NN)](PF$_6$) were synthesized and characterized in both solid state and solution. The compounds are analogues of previously reported Re(I) compounds and include NN polypyridyl phenanthroline or bipyridine derivatives along with Clotrimazole (CTZ) as bioactive ligands.

The compounds showed high activity against the infective trypomastigote form of *T. cruzi* and the promastigote form of *L. infantum* with EC$_{50}$ values in the low micromolar range and moderate selectivity index values tested using VERO cells as mammalian cell model. Compared with the previously reported Re(I) analogues, the Mn(I) compounds displayed EC$_{50}$ values of a similar magnitude against *T. cruzi* trypomastigotes but lower selectivity towards the parasite. In both metal families, incorporating two bioactive ligands into a single molecule mostly produced compounds with higher activities than the free ligands alone. Mn(I) compounds showed lower stability in three tested media compared with their Re(I) counterparts, losing at least in some extent the ligand CTZ. The Mn(I) compounds were more lipophilic than both the free bioactive ligands and the Re analogues, and no clear correlation was found between lipophilicity and antitrypanosomal activity, although the most active compound was also the most lipophilic of the series. Quantum chemical methods were employed to predict the water–octanol partition coefficients for both Re(I) and Mn(I) tricarbonyl complexes with varying polypyridine ligands and to explain the tendencies observed. Mn(I) compounds were found to be more lipophilic due to the Mn(I) center's higher polarizing power, which reduces the dipole moment by withdrawing electron density from donor atoms. Within each metal family, dipole moments were similar, with nonpolar surface contributions being more significant.

Metallomic study revealed an uptake of the most promising Mn compound, *fac*-[Mn(CO)$_3$(CTZ)(tmp)](PF$_6$), by *T. cruzi* more than twice that of the Re(I) compound and a preferential association to the soluble proteins fraction with negligible association to DNA for both compounds.

To elucidate the mechanism of action, potential targets such as DNA and CYP51 (lanosterol 14-α-demethylase), an enzyme critical for ergosterol biosynthesis, were investigated as well as structural changes induced by the compounds. Minimal DNA association (<1%) and moderate interaction with this target suggested that DNA binding is not the primary mechanism of action. In contrast, CYP51 inhibition was experimentally confirmed. Confocal Raman microscopy experiments suggested a possible disruption in the compartmentalization and localization of DNA within the parasite, which aligns with the changes expected for lipid metabolism and membrane dynamics. To further understand the mechanism of action of the most promising compound, *fac*-[M(CO)$_3$(CTZ)(tmp)](PF$_6$), in *T. cruzi*, the proteome of treated epimastigotes was analyzed. Proteomic analysis of epimastigotes treated with the Mn(I) and Re(I) compound showed no change in CYP51 abundance compared with untreated controls, suggesting that reduced ergosterol levels and accumulation of intermediates may arise from post-translational modifications of the enzyme. Additionally, altered abundances of methyltransferases, phosphatases, and kinases in treated parasites point to possible indirect modulation of ergosterol pathway proteins without changing their abundance. Furthermore, photoinduced CO

release was observed in Mn(I) tricarbonyls but not in their Re(I) analogues under the tested conditions. CO release in the dark triggered by other cell conditions may contribute to the biological activity and deserves further investigation. The activity against the parasites of the *fac*-[MnBr(CO)$_3$(NN)] precursors will be also explored along with the hypothesis of the new compounds acting as CTZ carriers, to provide new insight into the mechanism of action of the Mn(I) tricarbonyls.

Collectively, these results highlight the potential of Mn(I) and Re(I) tricarbonyls as promising candidates for further antitrypanosomal drug development.

Author contributions

Conceptualization: C. D. M., G. S., L. P. D., R. A. P., A. L., I. M., D. G. Validation: G. S., R. A. P., L. P. D., A. L., D. G. Formal analysis: C. D. M., G. S., A. L., L. P. D., I. M., N. V. Investigation: C. D. M., G. S., R. M., N. V., A. L., R. F., L. P. D., I. M. Resources: L. P. D., I. M., R. F., R. A. P., D. G. Writing original draft: C. D. M., L. P. D., A. L., D. G. Writing – review & editing: C. D. M., G. S., A. L., R. A. P., L. P. D., I. M., D. G. Visualization: D. G. Supervision: D. G. Project administration: D. G.

Data availability

The data supporting this article have been included as part of the ESI.†

Conflicts of interest

There are no conflicts of interest to declare.

Acknowledgements

C. D. M. acknowledges the support of the Agencia Nacional de Investigación e Innovación (ANII, Uruguay) through the Master grant POS_FCE_2021_1_1010807 and the Comisión Académica de Posgrado, UdelaR, Uruguay, PhD grant (BDDX_2024_1#49166839). The work was supported by Agencia Nacional de Investigación e Innovación (ANII, Uruguay) through the project grant FCE__2021_1_166665. CDM, RM, GS, DG thank PEDECIBA Uruguay. R. A. P. thanks CAPES (finance code 001), CAPES-PrInt, INCT-Catálise, FAPESC (2024TR002564), a FINEP for the financial support. R. A. P. thanks CNPq for the grant (309062/2023-3) and funding (404368/2023-9).

References

1 World Health Organisation, Neglected Tropical Diseases, **https://www.who.int/news-room/q-a-detail/neglected-tropical-diseases**, (accessed December 2024).
2 The Drugs for Neglected Diseases Initiative, Neglected Tropical Diseases, **https://dndi.org/diseases/neglected-tropical-diseases/#**, (accessed December 2024).
3 Y. C. Ong, S. Roy, P. C. Andrews and G. Gasser, *Chem. Rev.*, 2019, **119**, 730–796.
4 D. Gambino, *J. Braz. Chem. Soc.*, 2024, **35**, 1–21.
5 A. Yajima, Z. Lin, A. J. Mohamed, A. P. Dash and S. Rijal, *Lancet Regional Health – Southeast Asia*, 2023, **18**, 100302, DOI: **10.1016/j.lansea.2023.100302**.
6 P. J. Hotez, S. Aksoy, P. J. Brindley and S. Kamhawi, *PLoS Neglected Trop. Dis.*, 2020, **14**, 1–6.
7 I. Ribeiro, A. M. Sevcsik, F. Alves, G. Diap, R. Don, M. O. Harhay, S. Chang and B. Pecoul, *PLoS Neglected Trop. Dis.*, 2009, **3**, e84, DOI: **10.1371/journal.pntd.0000484**.
8 M. De Rycker, B. Baragaña, S. L. Duce and I. H. Gilbert, *Nature*, 2018, **559**, 498–506.
9 S. S. Santos, R. V. de Araújo, J. Giarolla, O. El Seoud and E. I. Ferreira, *Int. J. Antimicrob. Agents*, 2020, **55**, 105906.
10 V. Kourbeli, E. Chontzopoulou, K. Moschovou, D. Pavlos, T. Mavromoustakos and I. P. Papanastasiou, *Molecules*, 2021, **26**, 4629, DOI: **10.3390/molecules26154629**.
11 J. Brindha, M. M. Balamurali and K. Chanda, *Front. Chem.*, 2021, **9**, 622286, DOI: **10.3389/fchem.2021.622286**.
12 World Health Organisation, Chagas disease (American trypanosomiasis), **https://www.who.int/health-topics/chagas-disease** (accessed December 2024).
13 World Health Organisation, Leishmaniasis, **https://www.who.int/news-room/fact-sheets/detail/leishmaniasis**, (accessed September 2024).
14 M. Aslett, C. Aurrecoechea, M. Berriman, J. Brestelli, B. P. Brunk, M. Carrington, D. P. Depledge, S. Fischer, B. Gajria, X. Gao, M. J. Gardner, A. Gingle, G. Grant, O. S. Harb, M. Heiges, C. Hertz-Fowler, R. Houston, F. Innamorato, J. Iodice, J. C. Kissinger, E. Kraemer, W. Li, F. J. Logan, J. A. Miller, S. Mitra, P. J. Myler, V. Nayak, C. Pennington, I. Phan, D. F. Pinney, G. Ramasamy, M. B. Rogers, D. S. Roos, C. Ross, D. Sivam, D. F. Smith, G. Srinivasamoorthy, C. J. Stoeckert, S. Subramanian, R. Thibodeau, A. Tivey, C. Treatman, G. Velarde and H. Wang, *Nucleic Acids Res.*, 2010, **38**, D457–D462.
15 N. M. El-Sayed, P. J. Myler, G. Blandin, M. Berriman, J. Crabtree, G. Aggarwal, E. Caler, H. Renauld, E. A. Worthey, C. Hertz-Fowler, E. Ghedin, C. Peacock, D. C. Bartholomeu, B. J. Haas, A. Tran, J. R. Wortman, U. C. M. Alsmark, S. Angiuoli, A. Anupama, J. Badger, F. Bringaud, E. Cadag, J. M. Carlton, G. C. Cerqueira, T. Creasy, A. L. Delcher, A. Djikeng, T. Embley, C. Hauser, A. C. Ivens, S. K. Kummerfeld, J. B. Pereira-Leal, D. Nilsson, J. Peterson, S. L. Salzberg, J. Shallom, J. C. Silva, J. Sundaram, S. Westenberg, O. S. White, J. Donelson, B. Andersson, K. Stuart and N. Hall, *Science*, 2005, **309**, 404–409.
16 A. Ilari, I. Genovese, F. Fiorillo, T. Battista, I. De Ionna, A. Fiorillo and G. Colotti, *Mol. Pharm.*, 2018, **15**, 3069–3078.
17 K. Stuart, R. Brun, S. Croft, A. Fairlamb, R. E. Gürtler, J. McKerrow, S. Reed and R. Tarleton, *J. Clin. Invest.*, 2008, **118**, 1301–1310.

18 D. Gambino and L. Otero, *Front. Chem.*, 2022, **9**, 816266, DOI: **10.3389/fchem.2021.816266**.
19 D. Gambino and L. Otero, *Inorg. Chim. Acta*, 2018, **472**, 58–75.
20 D. Gambino and L. Otero, *Inorg. Chim. Acta*, 2012, **393**, 103–114.
21 D. Gambino, *Coord. Chem. Rev.*, 2011, **225**, 2193–2203.
22 J. Costa Pessoa, S. Etcheverry and D. Gambino, *Coord. Chem. Rev.*, 2015, **301**, 24–48.
23 R. W. Brown and C. J. T. Hyland, *MedChemComm*, 2015, **6**, 1230–1243.
24 M. Navarro, *Coord. Chem. Rev.*, 2009, **253**, 1619–1626.
25 D. Gambino and L. Otero, *Met. Ions Life Sci.*, 2019, 331–357, ch. 19.
26 R. A. Sánchez-Delgado, A. Anzelloti and L. Suárez, *Met. Ions Biol. Syst.*, 2004, **41**, 379–421.
27 M. Navarro, R. M. S. Justo, G. Y. S. Delgado and G. Visbal, *Curr. Pharm. Des.*, 2021, **27**, 1763–1789.
28 F. Rivas, C. Del Mármol, G. Scalese, L. Pérez-Díaz, I. Machado, O. Blacque, A. Medeiros, M. Comini and D. Gambino, *J. Inorg. Biochem.*, 2022, **237**, 112016, DOI: **10.1016/j.jinorgbio.2022.112016**.
29 M. Soba, G. Scalese, F. Casuriaga, N. Pérez, N. Veiga, G. A. Echeverría, O. E. Piro, R. Faccio, L. Pérez-Díaz, G. Gasser, I. Machado and D. Gambino, *Dalton Trans.*, 2023, **52**, 1623–1641.
30 F. Rivas, C. Del Mármol, G. Scalese, L. Pérez-Díaz, I. Machado, O. Blacque, F. Salazar, E. L. Coitiño, D. Benítez, A. Medeiros, M. Comini and D. Gambino, *Inorg. Chem.*, 2024, **63**, 11667–11687.
31 D. Gambino and L. Otero, *Met. Ions Life Sci.*, 2023, **24**, 193–214, ch. 7.
32 G. Scalese, I. Machado, F. Salazar, E. L. Coitiño, I. Correia, J. C. Pessoa, L. Pérez-Díaz and D. Gambino, *Front. Chem. Biol.*, 2024, **2**, 1304571, DOI: **10.3389/fchbi.2023.1304571**.
33 M. Soba, G. Scalese, L. Pérez-Díaz, D. Gambino and I. Machado, *Talanta*, 2022, **244**, 123413, DOI: **10.1016/j.talanta.2022.123413**.
34 G. Gasser, I. Ott and N. Metzler-Nolte, *J. Med. Chem.*, 2011, **54**(1), 3–25.
35 R. Alberto, R. Schibli, R. Waibel, U. Abram and A. P. Schubiger, *Coord. Chem. Rev.*, 1999, **190**, 901–919.
36 C. C. Konkankit, S. C. Marker, K. M. Knopf and J. J. Wilson, *Dalton Trans.*, 2018, **47**, 9934–9974.
37 S. Hostachy, C. Policar and N. Delsuc, *Coord. Chem. Rev.*, 2017, **351**, 172–188.
38 A. Leonidova and G. Gasser, *ACS Chem. Biol.*, 2014, **9**, 2180–2193.
39 E. B. Bauer, A. A. Haase, R. M. Reich, D. C. Crans and F. E. Kühn, *Coord. Chem. Rev.*, 2019, **393**, 79–117.
40 Y. Cortat, M. Nedyalkova, K. Schindler, P. Kadakia, G. Demirci, S. Nasiri Sovari, A. Crochet, S. Salentinig, M. Lattuada, O. M. Steiner and F. Zobi, *Antibiotics*, 2023, **12**, 619, DOI: **10.3390/antibiotics12030619**.
41 P. M. Toro, F. Peralta, J. Oyarzo, S. R. Wilkinson, M. Zavala, R. Arancibia, M. Moncada-Basualto, I. Brito, J. Cisterna, A. H. Klahn and C. López, *J. Inorg. Biochem.*, 2021, **219**, 111428.
42 I. Machado, S. Fernández, L. Becco, B. Garat, J. S. Gancheff, A. Rey and D. Gambino, *J. Coord. Chem.*, 2014, **67**, 1835–1850.
43 E. Rodríguez Arce, I. Machado, B. Rodríguez, M. Lapier, M. C. Zúñiga, J. D. Maya, C. Olea Azar, L. Otero and D. Gambino, *J. Inorg. Biochem.*, 2017, **170**, 125–133.
44 M. Patra, K. Ingram, V. Pierroz, S. Ferrari, B. Spingler, R. B. Gasser, J. Keiser and G. Gasser, *Chem. – Eur. J.*, 2013, **19**, 2232–2235.
45 A. C. R. Gonçalves, S. H. Libardi, J. C. Borges, R. J. Oliveira, C. Gotzmann, O. Blacque, S. de Albuquerque, C. D. Lopes, R. Alberto and P. I. S. Maia, *Dalton Trans.*, 2024, **53**, 19153–19165.
46 G. I. Lepesheva, L. Friggeri and M. R. Waterman, *Parasitology*, 2018, **145**, 1820–1836.
47 G. I. Lepesheva, F. Villalta and M. R. Waterman, *Adv. Parasitol.*, 2011, **75**, 65–87.
48 Y. Cortat and F. Zobi, *Pharmaceutics*, 2023, **15**, 2398, DOI: **10.3390/pharmaceutics15102398**.
49 A. Bencini and V. Lippolis, *Coord. Chem. Rev.*, 2010, **254**, 2096–2180.
50 G. Scalese, J. Benítez, S. Rostán, I. Correia, L. Bradford, M. Vieites, L. Minini, A. Merlino, E. L. Coitiño, E. Birriel, J. Varela, H. Cerecetto, M. González, J. C. Pessoa and D. Gambino, *J. Inorg. Biochem.*, 2015, **147**, 116–125.
51 J. Benítez, L. Guggeri, I. Tomaz, G. Arrambide, M. Navarro, J. Costa Pessoa, B. Garat and D. Gambino, *J. Inorg. Biochem.*, 2009, **103**, 609–616.
52 Z. Guo and P. J. Sadler, *Angew. Chem., Int. Ed.*, 1999, **38**, 1512–1531.
53 S. Kozieł, D. Wojtala, M. Szmitka, J. Sawka and U. K. Komarnicka, *Front. Chem. Biol.*, 2024, **3**, 1337372, DOI: **10.3389/fchbi.2024.1337372**.
54 F. Zobi, *Future Med. Chem.*, 2013, **5**(2), 175–188.
55 E. Kottelat and F. Zobi, *Inorganics*, 2017, **5**, 24, DOI: **10.3390/inorganics5020024**.
56 V. C. Weiss, G. Farias, A. L. Amorim, F. R. Xavier, T. P. Camargo, M. B. Bregalda, M. Haukka, E. Nordlander, B. De Souza and R. A. Peralta, *Inorg. Chem.*, 2020, **59**, 13078–13090.
57 A. L. Amorim, A. Guerreiro, V. A. Glitz, D. F. Coimbra, A. J. Bortoluzzi, G. F. Caramori, A. L. Braga, A. Neves, G. J. L. Bernardes and R. A. Peralta, *New J. Chem.*, 2020, **44**, 10892–10901.
58 S. S. Mendes, J. Marques, E. Mesterházy, J. Straetener, M. Arts, T. Pissarro, J. Reginold, A. Berscheid, J. Bornikoel, R. M. Kluj, C. Mayer, F. Oesterhelt, S. Friães, B. Royo, T. Schneider, H. Brötz-Oesterhelt, C. C. Romão and L. M. Saraiva, *ACS Bio Med Chem Au*, 2022, **2**, 419–436.
59 A. M. Mansour, R. M. Khaled and O. R. Shehab, *Dalton Trans.*, 2024, **53**, 19022–19057.
60 P. V. Simpson, C. Nagel, H. Bruhn and U. Schatzschneider, *Organometallics*, 2015, **34**, 3809–3815.

61 A. Jabłoński, K. Matczak, A. Koceva-Chyła, K. Durka, D. Steverding, K. Jakubiec-Krześniak, J. Solecka, D. Trzybiński, K. Woźniak, V. Andreu, G. Mendoza, M. Arruebo, K. Kochel, B. Krawczyk, D. Szczukocki and K. Kowalski, *Molecules*, 2017, **22**, 2220, DOI: **10.3390/molecules22122220**.
62 A. Toscani, C. Hind, M. Clifford, S. H. Kim, A. Gucic, C. Woolley, N. Saeed, K. M. Rahman, J. M. Sutton and D. Castagnolo, *Eur. J. Med. Chem.*, 2021, **213**, 113172.
63 N. C. Ammerman, M. Beier-Sexton and A. F. Azad, *Curr. Protoc. Microbiol.*, 2008, **11**(1), DOI: **10.1002/9780471729259.mca04es11**.
64 G. Scalese, I. Machado, G. Salinas, L. Pérez-Díaz and D. Gambino, *Molecules*, 2021, **26**, 5375, DOI: **10.3390/molecules26175375**.
65 M. Vieites, P. Smircich, B. Parajón-Costa, J. Rodríguez, V. Galaz, C. Olea-Azar, L. Otero, G. Aguirre, H. Cerecetto, M. González, A. Gómez-Barrio, B. Garat and D. Gambino, *J. Biol. Inorg. Chem.*, 2008, **13**, 723–735.
66 T. Mosmann, *J. Immunol. Methods*, 1983, **65**, 55–63.
67 S. Keller, Y. C. Ong, Y. Lin, K. Cariou and G. Gasser, *J. Organomet. Chem.*, 2020, **906**, 121059, DOI: **10.1016/j.jorganchem.2019.121059**.
68 F. Rivas, A. Medeiros, C. Quiroga, D. Benítez, M. Comini, E. Rodríguez-Arce, I. Machado, H. Cerecetto and D. Gambino, *Dalton Trans.*, 2021, **50**, 1651–1665.
69 C. M. Du, K. Valko, C. Bevan, D. Reynolds and M. H. Abraham, *Anal. Chem.*, 1998, **70**, 4228–4234.
70 L. Ayouni, G. Cazorla, D. Chaillou, B. Herbreteau, S. Rudaz, P. Lantéri and P. A. Carrupt, *Chromatographia*, 2005, **62**, 251–255.
71 J.-C. Chen and S. G. Weber, *J. Chromatogr. A*, 1982, **248**, 434–440.
72 M. R. Jones and B. R. Brooks, *J. Comput. Aided Mol. Des.*, 2020, **34**, 485–493.
73 K. S. A. M. Shweshein, F. Andrić, A. Radoičić, M. Zlatar, M. Gruden-Pavlović, Ž. Tešić and D. Milojković-Opsenica, *Sci. World J.*, 2014, **2014**, 862796, DOI: **10.1155/2014/862796**.
74 S. U. Dighe, S. Khan, I. Soni, P. Jain, S. Shukla, R. Yadav, P. Sen, S. M. Meeran and S. Batra, *J. Med. Chem.*, 2015, **58**, 3485–3499.
75 J. R. Lakowics, *Principles of Fluorescence Spectroscopy*, Springer Science, New York, 3rd edn, 2006, ch. 8, pp. 277–330.
76 F. Darabi, H. Hadadzadeh, M. Ebrahimi, T. Khayamian and H. A. Rudbari, *Inorg. Chim. Acta*, 2014, **409**, 379–389.
77 M. Santivañez-Veliz, E. Moreno-Viguri, S. Pérez-Silanes, J. Varela, H. Cerecetto, M. González and E. Lizarraga, *J. Chromatogr. B: Anal. Technol. Biomed. Life Sci.*, 2017, **1061–1062**, 225–232.
78 A. Gerpe, G. Álvarez, D. Benítez, L. Boiani, M. Quiroga, P. Hernández, M. Sortino, S. Zacchino, M. González and H. Cerecetto, *Bioorg. Med. Chem.*, 2009, **17**, 7500–7509.
79 V. C. Weiss, A. L. Amorim, F. R. Xavier, A. J. Bortoluzzi, A. Neves and R. A. Peralta, *J. Braz. Chem. Soc.*, 2019, **30**, 2649–2659.
80 M. F. Mosquillo, P. Smircich, A. Lima, S. A. Gehrke, G. Scalese, I. Machado, D. Gambino, B. Garat and L. Pérez-Díaz, *Bioinorg. Chem. Appl.*, 2020, 1634270, DOI: **10.1155/2020/1634270**.
81 J. Erde, R. R. O. Loo and J. A. Loo, *J. Proteome Res.*, 2014, **13**, 1885–1895.
82 M. D. M. Santos, D. B. Lima, J. S. G. Fischer, M. A. Clasen, L. U. Kurt, A. C. Camillo-Andrade, L. C. Monteiro, P. F. de Aquino, A. G. C. Neves-Ferreira, R. H. Valente, M. R. O. Trugilho, G. V. F. Brunoro, T. A. C. B. Souza, R. M. Santos, M. Batista, F. C. Gozzo, R. Durán, J. R. Yates III, V. C. Barbosa and P. C. Carvalho, *Nat. Protoc.*, 2022, **17**, 1553–1578.
83 X. Li, D. Zhang, G. Lu, G. Xiao, H. Chi, Y. Dong, Z. Zhang and Z. Hu, *J. Photochem. Photobiol., A*, 2012, **241**, 1–7.
84 A. M. Heyns, *Spectrochim. Acta, Part A*, 1977, **33**, 315–322.
85 W. J. Geary, *Coord. Chem. Rev.*, 1971, **7**, 81–122.
86 T. N. Thompson, *Med. Res. Rev.*, 2001, **21**, 412–449.
87 M. Starek, A. Plenis, M. Zagrobelna and M. Dąbrowska, *Pharmaceutics*, 2021, **13**, 440, DOI: **10.3390/pharmaceutics13040440**.
88 X. Liu, B. Testa and A. Fahr, *Pharm. Res.*, 2011, **28**, 962–977.
89 Z. Liu, T. Lu and Q. Chen, *Carbon*, 2021, **171**, 514–523.
90 J.-B. Lepecqt and A. C. Paoletti, *J. Mol. Biol.*, 1967, **27**, 87–106.
91 E. Rodríguez Arce, M. F. Mosquillo, L. Pérez-Díaz, G. A. Echeverría, O. E. Piro, A. Merlino, E. L. Coitiño, C. Maríngolo Ribeiro, C. Q. F. Leite, F. R. Pavan, L. Otero and D. Gambino, *Dalton Trans.*, 2015, **44**, 14453–14464.
92 F. Rivas, A. Medeiros, M. Comini, L. Suescun, E. Rodríguez Arce, M. Martins, T. Pinheiro, F. Marques and D. Gambino, *J. Inorg. Biochem.*, 2019, **199**, 110779, DOI: **10.1016/j.jinorgbio.2019.110779**.
93 B. Y. Wu, L. H. Gao, Z. M. Duan and K. Z. Wang, *J. Inorg. Biochem.*, 2005, **99**, 1685–1691.
94 G. Scalese, M. F. Mosquillo, L. Pérez-Díaz and D. Gambino, *Coord. Chem. Rev.*, 2024, **503**, 215608, DOI: **10.1016/j.ccr.2023.215608**.
95 F. S. Buckner and J. A. Urbina, *Int. J. Parasitol.: Drugs Drug Resist.*, 2012, **2**, 236–242.
96 K. Schindler and F. Zobi, *Molecules*, 2022, **27**, 593.
97 F. Ragone, J. G. Yañuk, F. M. Cabrerizo, E. Prieto, E. Wolcan and G. T. Ruiz, *J. Inorg. Biochem.*, 2024, **252**, 112471, DOI: **10.1016/j.jinorgbio.2023.112471**.
98 G. A. Zelada-Guillén, J. A. Ríos-Arce, M. A. Leyva-Peralta, M. Flores-Álamo, J. C. Gálvez-Ruíz, K. Calderón and M. V. Escárcega-Bobadilla, *Chem. Biodivers.*, 2023, **20**, e202200972.
99 T. K. Smith and P. Bütikofer, *Mol. Biochem. Parasitol.*, 2010, **172**, 66–79.
100 S. Sundar and B. Singh, *Expert Opin. Ther. Targets*, 2018, **22**, 467–486.
101 L. A. Booth and T. K. Smith, *Mol. Biochem. Parasitol.*, 2020, **240**, 111324, DOI: **10.1016/j.molbiopara.2020.111324**.